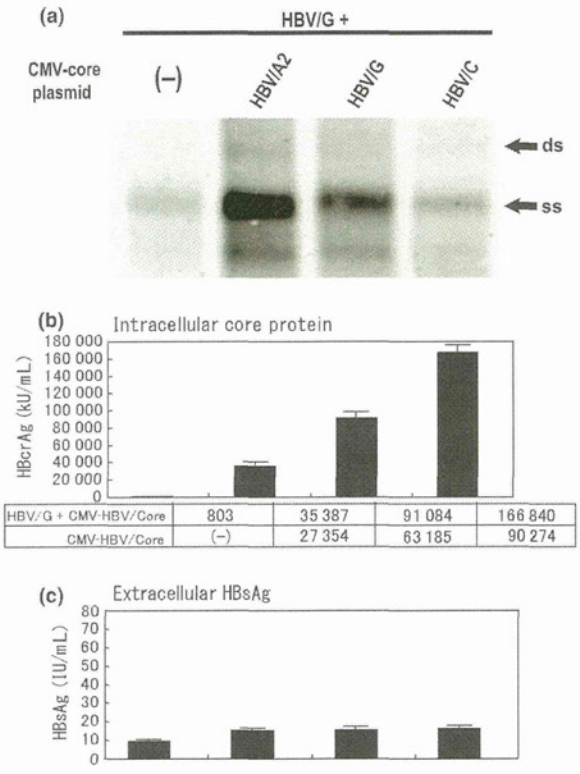

Fig. 4 (a) Southern blot analysis for the expression of intracellular HBV/G DNA during co-transfection with the three core protein expression constructs for each genotype (HBV/G, HBV/A2 and HBV/C) driven by the CMV promoter, which produced core protein in the absence of a preceding ε signal. (b) Intracellular expression of core protein. (c) The expression of HBsAg in the culture supernatant.

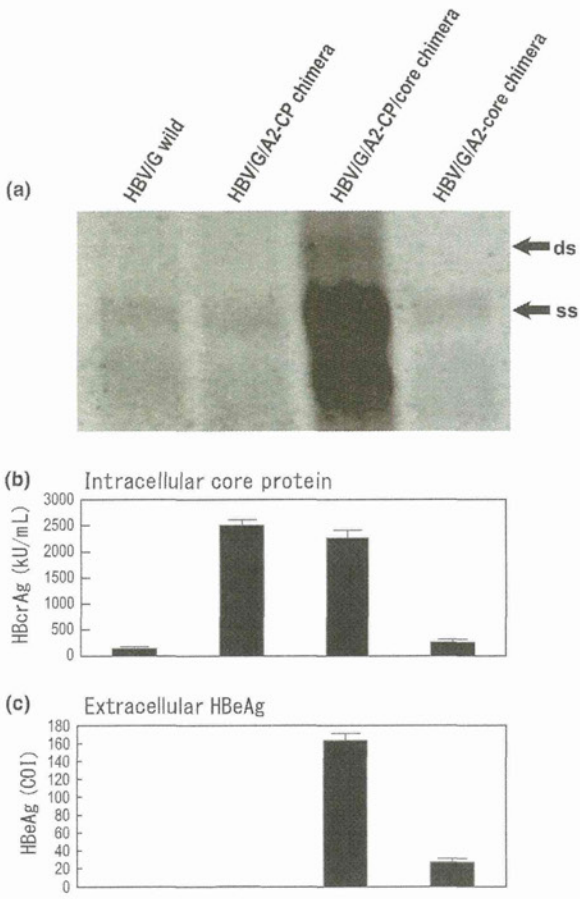

Fig. 5 (a) Southern blot analysis for HBV replication among HBV/G and three chimeric replicating constructs created by recombination of different genomic sections of HBV/G and HBV/A2 (see Materials and methods). The 'HBV/G/A2-CP' clone was a HBV/G-based construct in which the fragment containing the core promoter (CP) region but not the precore or core was replaced by the corresponding sequence from HBV/A2. The 'HBV/G/A2-Core' clone was an HBV/G-based construct in which the section of the precore and core region was replaced with that of HBV/A2. For the 'HBV/G/A2-CP/core' clone, the CP, precore and core region of HBV/G were replaced with that of HBV/A2. (b) Intracellular expression of core protein. (c) Extracellular expression of HBeAg levels detected by a commercial chemiluminescent enzyme immunoassay (mean and standard deviation, $n = 3$).

levels of core protein (HBcrAg) expression were observed for the HBV/G/A2-CP and HBV/G/A2-CP/core-transfected cultures, which was in sharp contrast with the low levels observed in the HBV/G/A2-core and the wild-type HBV/G cultures. The discrepancy between viral replication and core production of the HBV/G/A2-CP clone might indicate insufficient virion assembly. Figure 5c shows the HBeAg levels measured in culture supernatants. The expression of HBeAg was the highest in the HBV/G/A2-CP/core culture distantly followed by that in the HBV/G/A2-core culture. The HBV/G/A2-CP and wild-type HBV/G clones expressed HBeAg protein at levels close to or below the level of detection. Nevertheless, a high HBcrAg titre was detected in the cell lysate of the HBV/G/A2-CP clone, although its DNA level was as low as that of the wild-type HBV/G clone (Fig. 5a). These results indicated that low replication of HBV/G might be explained by low synthesis of HBV/G core protein due to weak core promoter activity or dysfunction, as well as insufficient virion assembly due to the larger core protein of HBV/G (12-aa unique insertion).

Dane particles produced by HBV/G during co-transfection with HBV/A2 were packed in HBV/A2 protein

To investigate the effects of HBV/A2 core protein during HBV/G viral assembly, we tried to define whether the Dane particles in B Huh7 cells that had been co-transfected with wild-type HBV/G and the CMV-HBV/A2-core plasmid

(source of the Fig. 4 lane 2) contained HBV/A2 or HBV/G core protein. To extract the Dane particles, we employed ultracentrifugation of the culture media through a 10–60% (w/w) sucrose density gradient followed by immunoprecipitation using anti-HBs-coated magnetic beads. We thereby extracted Dane particles, which were then analysed using Western blotting. The obtained fractions were tested for HBcrAg, HBsAg and HBV DNA (Fig. 6a). HBcrAg appeared in the high-density fractions, and its levels peaked in the same fraction (fraction 22) as HBV DNA. As reported previously, the fraction in which the levels of HBV DNA and HBcrAg peaked contained Dane particles [22]. To eliminate contamination of the Dane particles with 'naked' core particles or core protein, they were specifically retrieved from sucrose high-density fraction 22 by means of immunoprecipitation using anti-HBs-coated magnetic beads. The media supernatant obtained from the culture of cells that had been subjected to CMV-HBV/A2/core clone monotransfection was also subjected to sucrose gradient ultracentrifugation using the same protocol. Sucrose high-density fraction 22, in which the HBcrAg concentration peaked, presumably contained 'naked' core particles or core protein (Fig. 6b). This fraction was collected and processed in the same manner via anti-HBs-coated magnetic bead separation and was used as negative control for this procedure (Fig. 6c, lane 4). To discriminate between HBV/G and HBV/A2 core proteins on Western blot analysis probed with anti-HBc antibody, we employed cell lysates produced from cells that had been transfected with the wild-type HBV/G clone and those produced with the HBV/A2 clone as controls. As can be seen on the Western blotting image (Fig. 6c), HBV/G-transfected cells (lane 1) produced larger proteins than the HBV/A2-transfected cells (lane 2), which can be explained by the 12-aa insertion in the core protein of HBV/G coded by its 36-nt unique insertion. Interestingly, the most saturated band associated with the Dane particles produced by HBV/G that had been co-transfected with CMV-HBV/A2/core (lane 3) was the same size as that for HBV/A2, suggesting that HBV/G competitively produces Dane particles consisting of HBV/A2 core protein during virion assembly.

DISCUSSION

HBV/G was first isolated in 2000 in France and the USA and was later found in Thailand, Japan and Mexico, indicating its global dissemination and association with specific risk groups, such as injection drug users (IDU) and men who had sex with men (MSM) [25]. Studies have also demonstrated that throughout the world, HBV/G strains possess unprecedented genetic homology and are mainly detected during co-infection with another genotype that is endemic in the area. Further studies have suggested that genotype G represents a 'replication-defective' variant of HBV that requires co-infection with another genotype to establish a persistent infection. We and others have reported *in vitro* and *in vivo* experimental evidence of this HBV/G dependence [13–15]. The unique 36-nt insertion within core coding region increases core protein level and genome replication in genotype G but impairs replication, not core protein expression, in other genotypes [14]. These results strongly suggest the 36-nt/12-aa insertion has pleiotropic effects on core protein expression, genome replication and virion secretion [14]. To obtain clues about the mechanism by which genotype G works in combination with genotype A to effect its replication, we performed co-transfection experiments using Huh7 cells.

Using HBV/A2 viral proteins expressing plasmids, we determined that a HBV/A2 plasmid that selectively expressed core protein was capable of increasing the replication of the wild-type HBV/G (Fig. 3a). The replication of HBV/G during co-transfection was not affected by other viral elements of HBV/A2 because of the presence of the 'packaging-negative mutation' in the epsilon-coding region and stop codons preventing the translation of the other three viral proteins (the polymerase, surface and X proteins). The specific role of the core protein was further confirmed in experiments with CMV promoter–driven core expressing constructs, in which the core protein alone enhanced HBV/G replication in the absence of HBV pregenomic RNA. Interestingly, co-transfection of HBV/G with the CMV-HBV/A2/core expression construct produced the highest levels of intracellular DNA, even though this combination produced the lowest intracellular core protein level, compared with the CMV-core constructs of the other two genotypes (HBV/G and HBV/C) (Figs 4a,b). The replication of HBV/G was the highest during co-transfection with the CMV-HBV/A2/core expression construct, which agreed with the results of experiments using other genotype (HBV/D, HBV/B1) CMV-core constructs (data not shown). Thus, the core protein of HBV/A2 was confirmed to play an important role in upregulating HBV/G replication and performed this task more efficiently than the other genotypes. These experimental results might explain why HBV/A is the genotype that is most frequently found in co-infections with HBV/G [12,26].

Moreover, HBV/G core protein overexpression achieved by the co-transfection of HBV/G with CMV-HBV/G/core did not enhance replication, suggesting that HBV/G core protein is functionally defective; that is, results in insufficient viral packaging. To investigate the functional defect in the HBV/G core protein, we exchanged the core gene of the wild-type HBV/G for the corresponding gene of HBV/A2 (HBV/G/A2-core); the introduction of the HBV/A2 core promoter together with core coding region into the HBV/G genome (HBV/G/A2-CP/core) significantly enhanced replication. However, the replication of the recombinant construct (HBV/A2 core coding region; HBV/G/A2-core) did not differ from that of the wild-type HBV/G, suggesting that the replacement of HBV/G/A2-core alone was not

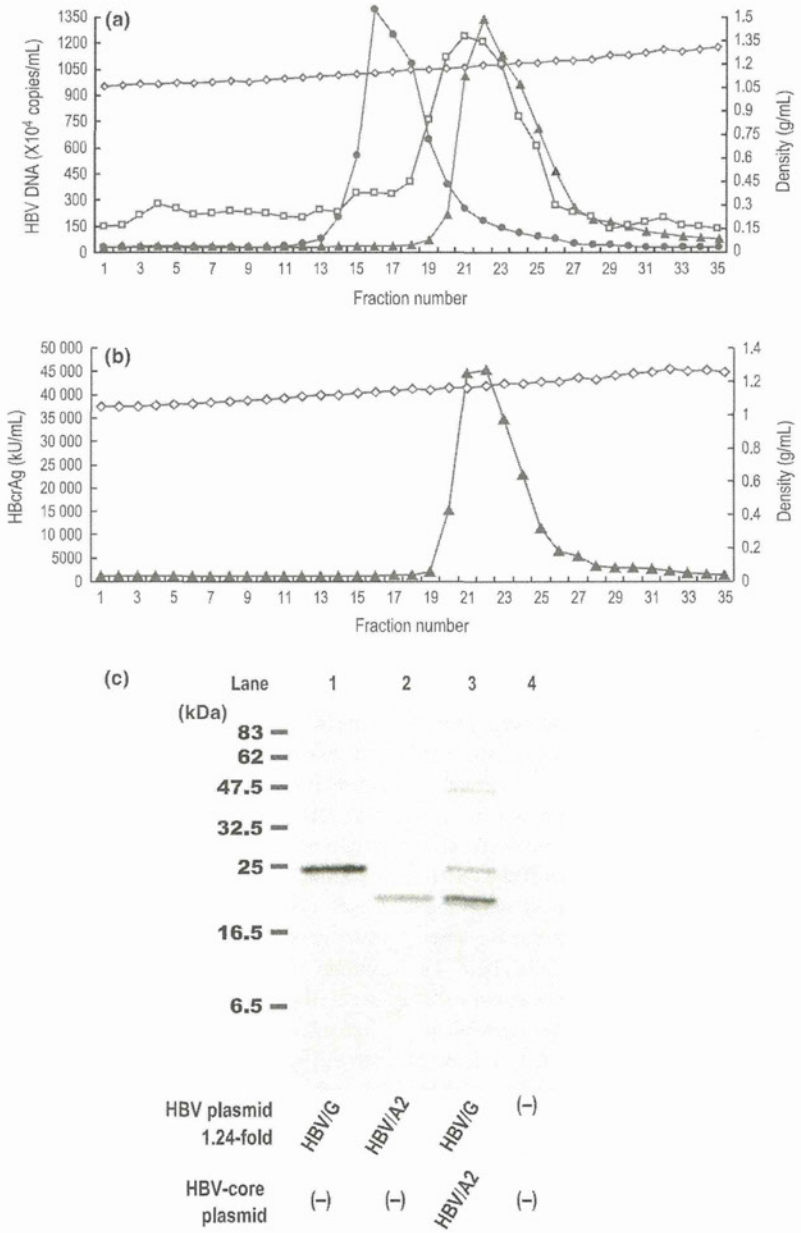

Fig. 6 (a) Sucrose gradient analysis of the culture media of Huh7 cells that had been co-transfected with wild-type HBV/G and the CMV-HBV/A2-core plasmid. It was subjected to ultracentrifugation through a 10–60% (w/w) sucrose density gradient. Density of each fraction is shown as a line with diamond symbols. Fractions were diluted 10-fold and tested for HBsAg (●) (IU/mL), HBcrAg (▲) (KU/mL) and HBV DNA (□) (10^4 copies/mL). (b) Sucrose gradient analysis of culture supernatant obtained from the cells that were subjected to CMV-HBV/A2/core monotransfection using the same protocol. (c) Western blot analysis for HBV core protein was probed by anti-HBc antibody. HBV/G/core and HBV/A2/core were obtained from cell lysates that were transfected with the wild-type HBV/G clone and the wild-type HBV/A2 clone, respectively. The 'HBV/G + CMV-HBV/A2/core' was obtained from sucrose high-density fraction 22 (Fig. 6a) that had been co-transfected with wild-type HBV/G and the CMV-HBV/A2-core plasmid by means of immunoprecipitation using anti-HBs-coated magnetic beads.

enough for viral replication because the core promoter of HBV/G was not capable of generating sufficient amounts of core protein to enhance HBV replication. As well, an HBV/G/A2-CP construct containing the HBV/A core promoter region in the context of the wild-type HBV/G genome did not enhance replication, even though its core protein

production was significantly increased (Figs 5a,b). Although it was previously reported that the 36-nt insertion of the HBV/G core gene was required for both efficient core protein expression and HBV/G replication [13], in this study, the discrepancy between viral replication and core production of the HBV/G/A2-CP clone might indicate insufficient virion assembly due to the larger core protein of HBV/G (12-aa unique insertion). *Trans*-complementation experiments carried out by Gutelius *et al.* [14] demonstrated an association between enhanced core protein level and reduced replication capacity only when the core and polymerase proteins are expressed from the same RNA template. Thus, it was indicated that HBV/G itself could not replicate sufficiently due to a defect in its core protein and/or the core promoter of HBV/G.

Finally, we investigated whether HBV/G utilises the core protein of HBV/A2 for virion packaging. Dane particles obtained from the culture supernatants of cells that had been co-transfected with HBV/G and CMV-HBV/A2/core were assessed by Western blotting, and it was found that the Dane particles of HBV/G contained HBV/A core proteins. Thus, it was implied that HBV/G replication is enhanced by the core protein of HBV/A because it is more suitable for virion packaging than its own core protein, suggesting that the core protein of HBV/A is a key element enhancing the replication of HBV/G during co-infection. Interestingly, our experiments demonstrated that there were large differences in core protein expression among the CMV-core constructs of different genotypes, despite the fact that all of the CMV-core constructs had the same CMV promoter (Fig. 4b). In a previous report, it was speculated that the core protein binds to its own mRNA to influence protein translation [13]. For example, dihydrofolate reductase protein has been found to downregulate its own translation by binding to cognate mRNA [27,28]. Therefore, we predict that the core protein of HBV/A2 enhances HBV/G replication by affecting viral promoters or transcription in addition to its role in virion packaging.

In conclusion, enhanced replication of HBV/G requires the HBV/A2 core protein during co-infection with HBV/A2. Our findings provide a possible explanation that the core protein of HBV/A2 is more suitable for virion packaging rather than that of HBV/G, and the replication of HBV/G occurs at a very low level, which may be due to defects in its core protein functions and/or core promoter activity. Further experiments are warranted to clarify the detailed roles of the enhanced HBV/G replication by co-infection with the other genotype and the clinical manifestation of HBV/G infection.

ACKNOWLEDGEMENTS

This study was supported, in part, by a grant-in-aid from the Ministry of Health, Labour and Welfare of Japan and a grant-in-aid from the Ministry of Education, Culture, Sports, Science and Technology. We thank Ms H. Naganuma of Nagoya City University Graduate School of Medical Sciences, Nagoya, Japan, for doing serological assays.

CONFLICT OF INTEREST STATEMENT

None declared.

REFERENCES

1 Kao JH, Chen DS. Global control of hepatitis B virus infection. *Lancet Infect Dis* 2002; 2(7): 395–403. Epub 2002/07/20.
2 Kim BK, Revill PA, Ahn SH. HBV genotypes: relevance to natural history, pathogenesis and treatment of chronic hepatitis B. *Antivir Ther* 2011; 16(8): 1169–1186. Epub 2011/12/14.
3 Okamoto H, Tsuda F, Sakugawa H, Sastrosoewignjo RI, Imai M, Miyakawa Y *et al.* Typing hepatitis B virus by homology in nucleotide sequence: comparison of surface antigen subtypes. *J Gen Virol* 1988; 69 (Pt 10): 2575–2583. Epub 1988/10/01.
4 Norder H, Courouce AM, Magnius LO. Complete genomes, phylogenetic relatedness, and structural proteins of six strains of the hepatitis B virus, four of which represent two new genotypes. *Virology* 1994; 198(2): 489–503. Epub 1994/02/01.
5 Orito E, Ichida T, Sakugawa H, Sata M, Horiike N, Hino K *et al.* Geographic distribution of hepatitis B virus (HBV) genotype in patients with chronic HBV infection in Japan. *Hepatology* 2001; 34(3): 590–594. Epub 2001/08/30.
6 Stuyver L, De Gendt S, Van Geyt C, Zoulim F, Fried M, Schinazi RF *et al.* A new genotype of hepatitis B virus: complete genome and phylogenetic relatedness. *J Gen Virol* 2000; 81(Pt 1): 67–74. Epub 2000/01/21.
7 Kato H, Orito E, Gish RG, Bzowej N, Newsom M, Sugauchi F *et al.* Hepatitis B e antigen in sera from individuals infected with hepatitis B virus of genotype G. *Hepatology* 2002; 35(4): 922–929. Epub 2002/03/27.
8 Osiowy C, Gordon D, Borlang J, Giles E, Villeneuve JP. Hepatitis B virus genotype G epidemiology and co-infection with genotype A in Canada. *J Gen Virol* 2008; 89(Pt 12): 3009–3015. Epub 2008/11/15.
9 Suwannakarn K, Tangkijvanich P, Theamboonlers A, Abe K, Poovorawan Y. A novel recombinant of hepatitis B virus genotypes G and C isolated from a Thai patient with hepatocellular carcinoma. *J Gen Virol* 2005; 86(Pt 11): 3027–3030. Epub 2005/10/18.
10 Sanchez LV, Tanaka Y, Maldonado M, Mizokami M, Panduro A. Difference of hepatitis B virus genotype distribution in two groups of Mexican

patients with different risk factors. High prevalence of genotype H and G. *Intervirology* 2007; 50(1): 9–15. Epub 2006/12/14.

11 Tanaka Y, Sanchez LV, Sugiyama M, Sakamoto T, Kurbanov F, Tatematsu K *et al.* Characteristics of hepatitis B virus genotype G coinfected with genotype H in chimeric mice carrying human hepatocytes. *Virology* 2008; 376(2): 408–415. Epub 2008/05/14.

12 Kato H, Orito E, Gish RG, Sugauchi F, Suzuki S, Ueda R *et al.* Characteristics of hepatitis B virus isolates of genotype G and their phylogenetic differences from the other six genotypes (A through F). *J Virol* 2002; 76(12): 6131–6137. Epub 2002/05/22.

13 Li K, Zoulim F, Pichoud C, Kwei K, Villet S, Wands J *et al.* Critical role of the 36-nucleotide insertion in hepatitis B virus genotype G in core protein expression, genome replication, and virion secretion. *J Virol* 2007; 81(17): 9202–9215. Epub 2007/06/15.

14 Gutelius D, Li J, Wands J, Tong S. Characterization of the pleiotropic effects of the genotype G-specific 36-nucleotide insertion in the context of other hepatitis B virus genotypes. *J Virol* 2011; 85(24): 13278–13289. Epub 2011/10/14.

15 Sugiyama M, Tanaka Y, Sakamoto T, Maruyama I, Shimada T, Takahashi S *et al.* Early dynamics of hepatitis B virus in chimeric mice carrying human hepatocytes monoinfected or coinfected with genotype G. *Hepatology* 2007; 45(4): 929–937. Epub 2007/03/30.

16 Lacombe K, Massari V, Girard PM, Serfaty L, Gozlan J, Pialoux G *et al.* Major role of hepatitis B genotypes in liver fibrosis during coinfection with HIV. *AIDS* 2006; 20(3): 419–427. Epub 2006/01/28.

17 Sugiyama M, Tanaka Y, Kato T, Orito E, Ito K, Acharya SK *et al.* Influence of hepatitis B virus genotypes on the intra- and extracellular expression of viral DNA and antigens. *Hepatology* 2006; 44(4): 915–924. Epub 2006/09/29.

18 Bruss V, Ganem D. The role of envelope proteins in hepatitis B virus assembly. *Proc Natl Acad Sci U S A* 1991; 88(3): 1059–1063. Epub 1991/02/01.

19 Tang H, Delgermaa L, Huang F, Oishi N, Liu L, He F *et al.* The transcriptional transactivation function of HBx protein is important for its augmentation role in hepatitis B virus replication. *J Virol* 2005; 79(9): 5548–5556. Epub 2005/04/14.

20 Pollack JR, Ganem D. An RNA stem-loop structure directs hepatitis B virus genomic RNA encapsidation. *J Virol* 1993; 67(6): 3254–3263. Epub 1993/06/01.

21 Ozasa A, Tanaka Y, Orito E, Sugiyama M, Kang JH, Hige S *et al.* Influence of genotypes and precore mutations on fulminant or chronic outcome of acute hepatitis B virus infection. *Hepatology* 2006; 44(2): 326–334. Epub 2006/07/28.

22 Kimura T, Ohno N, Terada N, Rokuhara A, Matsumoto A, Yagi S *et al.* Hepatitis B virus DNA-negative Dane particles lack core protein but contain a 22-kDa precore protein without C-terminal arginine-rich domain. *J Biol Chem* 2005; 280(23): 21713–21719. Epub 2005/04/09.

23 Fujiwara K, Tanaka Y, Paulon E, Orito E, Sugiyama M, Ito K *et al.* Novel type of hepatitis B virus mutation: replacement mutation involving a hepatocyte nuclear factor 1 binding site tandem repeat in chronic hepatitis B virus genotype E. *J Virol* 2005; 79(22): 14404–14410. Epub 2005/10/29.

24 Orchard S, Martens L, Tasman J, Binz PA, Albar JP, Hermjakob H. 6th HUPO Annual World Congress – Proteomics Standards Initiative Workshop 6–10 October 2007, Seoul, Korea. *Proteomics* 2008; 8(7): 1331–1333. Epub 2008/03/05.

25 Kurbanov F, Tanaka Y, Mizokami M. Geographical and genetic diversity of the human hepatitis B virus. *Hepatol Res* 2010; 40(1): 14–30. Epub 2010/02/17.

26 Osiowy C, Giles E. Evaluation of the INNO-LiPA HBV genotyping assay for determination of hepatitis B virus genotype. *J Clin Microbiol* 2003; 41(12): 5473–5477. Epub 2003/12/10.

27 Chu E, Takimoto CH, Voeller D, Grem JL, Allegra CJ. Specific binding of human dihydrofolate reductase protein to dihydrofolate reductase messenger RNA in vitro. *Biochemistry* 1993; 32(18): 4756–4760. Epub 1993/05/11.

28 Ercikan-Abali EA, Banerjee D, Waltham MC, Skacel N, Scotto KW, Bertino JR. Dihydrofolate reductase protein inhibits its own translation by binding to dihydrofolate reductase mRNA sequences within the coding region. *Biochemistry* 1997; 36(40): 12317–12322. Epub 1997/10/07.

SUPPORTING INFORMATION

Additional Supporting Information may be found in the online version of this article:

Data S1. Plasmid construct of HBV/G.

SCIENTIFIC REPORTS

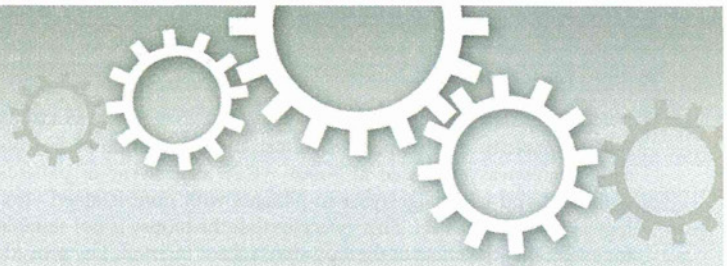

OPEN

SUBJECT AREAS:
GLYCOBIOLOGY
BIOCHEMICAL ASSAYS
ASSAY SYSTEMS
ELISA

Received
3 September 2012

Accepted
27 December 2012

Published
15 January 2013

Correspondence and requests for materials should be addressed to H.N. (h.narimatsu@aist.go.jp)

* These authors contributed equally to this study.

A serum "sweet-doughnut" protein facilitates fibrosis evaluation and therapy assessment in patients with viral hepatitis

Atsushi Kuno[1]*, Yuzuru Ikehara[1]*, Yasuhito Tanaka[2], Kiyoaki Ito[3], Atsushi Matsuda[1], Satoru Sekiya[1], Shuhei Hige[4], Michiie Sakamoto[5], Masayoshi Kage[6], Masashi Mizokami[3] & Hisashi Narimatsu[1]

[1]Research Center for Medical Glycoscience (RCMG), National Institute of Advanced Industrial Science and Technology (AIST), Tsukuba, Japan, [2]Department of Virology & Liver Unit, Nagoya City University Graduate School of Medical Sciences, Nagoya, Japan, [3]The Research Center for Hepatitis and Immunology, National Center for Global Health and Medicine, Ichikawa, Japan, [4]Department of Internal Medicine, Hokkaido University Graduate School of Medicine, Sapporo, Japan, [5]Department of Pathology, School of Medicine, Keio University, Tokyo, Japan, [6]Department of Pathology, Kurume University School of Medicine, Kurume, Japan.

Although liver fibrosis reflects disease severity in chronic hepatitis patients, there has been no simple and accurate system to evaluate the therapeutic effect based on fibrosis. We developed a glycan-based immunoassay, FastLec-Hepa, to fill this unmet need. FastLec-Hepa automatically detects unique fibrosis-related glyco-alteration in serum hyperglycosylated Mac-2 binding protein within 20 min. The serum FastLec-Hepa counts increased with advancing fibrosis and illustrated significant differences in medians between all fibrosis stages. FastLec-Hepa is sufficiently sensitive and quantitative to evaluate the effects of PEG-interferon-α/ribavirin therapy in a short post-therapeutic interval. The obtained fibrosis progression is equivalent to -0.30 stages/year in patients with sustained virological response, and 0.01 stages/year in relapse/nonresponders. Furthermore, long-term follow-up of the severely affected patients found hepatocellular carcinoma developed in patients after therapy whose FastLec-Hepa counts remained above a designated cutoff value. FastLec-Hepa is the only assay currently available for clinically beneficial therapy evaluation through quantitation of disease severity.

The World Health Organization has estimated that the prevalence of chronic infections with hepatitis B virus (HBV) and hepatitis C virus (HCV) is more than 5% of the world population. The high rate of viral transmission worldwide has also resulted in an explosive increase in incidence of liver cirrhosis (LC), because liver fibrosis caused by the persistent infections with HBV and HCV irreversibly progresses in chronic hepatitis (CH) patients without effective treatment. As the incidence of hepatocellular carcinoma (HCC) increases proportionally to the severity of hepatitis and the presence of LC, it is now clear that about 90% of HCC cases originate from infection with HBV or HCV. It is estimated that more than one million patients worldwide die from liver disease related to HBV or HCV infection each year. Immunomodulatory therapy with PEG-interferon-α and ribavirin is the standard treatment for patients with chronic hepatitis C (CHC)[1]. Recent genome-wide association studies have revealed that variation in the host interleukin-28B gene can predict the outcome of therapies for viral clearance[2–4]. Such pharmacokinetic understanding should allow for more precise treatment protocols and follow-up analyses to optimize the opportunity for patients to achieve sustained virological response (SVR)[5,6]. Linear peptidomimetic HCV and NS3/4A serine protease inhibitors such as telaprevir and boceprevir are new drugs that, in combination with PEG-interferon-α and ribavirin, substantially improve the rates of response among patients with HCV genotype 1 infection[1]. Alternatively, suppression of hepatic decompensation in chronic hepatitis B patients with advanced fibrosis and cirrhosis has been evaluated during long-term treatment with antiviral agents, such as adefovir, lamivudine, entecavir, and tenofovir[7]. For example, cumulative entecavir therapy (for at least 3 years) resulted in substantial histological improvement and regression of fibrosis or cirrhosis[8].

The efficacy of therapy is currently evaluated by frequent monitoring of "viral load" or "liver injury"[5]. From the viewpoint of developing preventive strategies for HCC, the risk of HCC development should also be estimated along with them. For this purpose, liver biopsy is generally considered as the gold standard in which fibrosis is subclassified into 5 stages of severity (F0–4). However, this procedure is invasive and shown to cause a high rate of sampling error (about 15% false-negatives for cirrhosis) in patients with diffuse parenchymal liver diseases.

Furthermore, in a retrospective cohort study[9], the rate of fibrosis progression was estimated at about −0.28 stages/year in patients with SVR and 0.02 stages/year in patients with nonsustained virological response (NVR). This indicates that the biopsy is not suitable for evaluating the effect of therapy after a short interval. The procedure has further disadvantages such as inaccuracy, biopsy-related complications, the need for hospitalization, the time involved, and low cost-effectiveness[10]. Therefore, alternative noninvasive assays are desired and should provide a quantifiable readout of fibrosis progression using a method that is accurate, cost-effective and relatively simple.

To date, several methods have been developed[10] including FibroScan, which measures hepatic fibrosis biomechanically as tissue stiffness based on transient elastography. FibroScan has the advantages of being rapid and technically simple; however, its diagnostic success rate is affected by operator skill. Therefore, it has been suggested that FibroScan, in conjunction with assay of serum fibrosis biomarkers, should improve diagnostic accuracy. FibroTest[11] and FibroMeter[12], believed to be the most reliable indices of fibrosis, have been used in the combination assay aiming to eliminate the need for liver biopsy[13,14]. However, FibroTest and FibroMeter do not complement FibroScan in the development of a rapid "on-site diagnosis" system. This is because each requires both extensive and specialized blood analyses (FibroTest requires α2-macroglobulin, apolipoprotein A1, haptoglobin, γ-glutamyltransferase and total bilirubin whereas FibroMeter requires platelet count, prothrombin index, AST, α2-macroglobulin, hyaluronic acid and urea). In addition, both tests require data on age, and also sex for FibroTest.

Glycans are referred to as the face of cells, which reflect their status such as differentiation stage rather than their state of damage, and therefore they can be great markers for chronic disease. In the case of hepatitis, glycans are considered to reflect more specifically the progression of fibrosis than viral load. In the search for a simple and rapid method that is not markedly affected by tissue inflammation and ALT fluctuation, the possibility of glycomic and glycoproteomic techniques has emerged[15,16], and there are reports of some successful examples applicable for use in the clinical laboratories[17–19]. However, the current glycomic techniques require at least 3 hours of sample preparation for analysis and this has markedly reduced the combination use of glycan-based immunoassays with FibroScan. In this report, we describe for the first time, a rapid and simple glycan-based immunoassay, FastLec-Hepa, that can quantify fibrosis as precisely as FibroTest and also readily evaluate the antifibrotic effects of therapy at the clinical site (**Supplementary Fig. 1**). Moreover, we introduce a novel method for rational selection of the "non-fucose binding type" lectins and provide details of how this concept can be adopted for future development of clinically useful glycodiagnostic tools.

Results

Changes in the *N*-glycosylation of M2BP during progression of liver disease. Based on previous reports[20–23], we adopted the serum 90 K/Mac-2 binding protein (M2BP) as a glycoprotein biomarker for liver fibrosis. M2BP is secreted from many cell types, including hepatocytes (http://www.proteinatlas.org/ENSG00000108679), and it has been shown to modulate many processes, particularly those related to cell adhesion. For example, the interaction of M2BP with matrix fibronectin can modulate adhesion and the high expression of M2BP by tumor cells increases the level in the circulation of affected patients. A prominent feature of native human M2BP is its oligomerization to large ring structures[20], resembling a "sugar-powdered doughnut" which is potentially covered with 70–112 *N*-glycans (**Fig. 1a**). To confirm serum M2BP as a valid marker, we performed a pull-down assay with serum (2 μl each) from five individuals in each of the following groups: HCC, LC, CHC or healthy volunteer with normal liver (HV). Although two bands appeared in all HVs and two CHC patients, M2BPs from patients with relatively severe fibrosis, i.e., LC and HCC, migrated as a single band, the mobility of which was similar to that of the lower band for HVs (**Fig. 1b**). Significant increases in band intensity with excessive smearing of the bands were seen for most HCC patients. A subsequent investigation of 125 HCV patients with stage-determined fibrosis showed alteration in the quality and quantity of M2BP during the progression of fibrosis (**Fig. 1c**) and apparent alteration in the amount of each band (**Fig. 1d and e**), as described in the previous investigations[22,23]. M2BP has been shown to have multibranching and sialylated *N*-glycans. Moreover, it has been suggested that extension of polylactosamine on M2BP controls its binding to galectin-3, a major binding partner *in vivo*. Sialylation and extension of polylactosamine affect the charge and size of M2BP and this results in altered electrophoretic migration. Accordingly, we speculate that the size heterogeneity of M2BP seen on electrophoresis is due to such alterations in glycosylation. In fact, the difference in the band migration was eliminated by Sialidase A treatment, and the smearing of the bands in HCC was reduced by treatment with *N*-Glycosidase F (**Supplementary Fig. 2**). These results indicated that the altered quality of M2BP during progression of liver disease was due to changes in *N*-glycosylation.

Selection of the optimal lectin for direct measurement of disease-related M2BP. To construct a reliable assay (see **Supplementary Fig. 3**), we needed to identify a lectin probe that could most readily discriminate the altered *N*-glycans of M2BP and specifically binds to them in serum without pretreatment. For this purpose, we added a subtraction process to our recently described microarray-based selection strategy[16] (**Supplementary Fig. 4**). In brief, we first obtained a typical glycan profile for serum M2BPs by averaging the glycan profiles of M2BPs immunoprecipitated from 125 HCV patient sera by the antibody-overlay lectin microarray[16,18,24] (**step 1**). In this step, we selected 27 lectins binding to M2BP from a 45-lectin array (**Supplementary Fig. 5a**). Most of them bound not only to M2BP (ca. 10 μg/ml in serum), but also to other abundant serum glycoproteins, whereas some suggested rather specific binding to M2BP. We designated them as high-noise lectins or high signal-to-noise (S/N) lectins, respectively (**Fig. 2a**). We then selected the candidate lectins for the assay by subtracting the high-noise lectins from the M2BP-binding lectins (**step 2**), using a glycan profile of whole serum (**Supplementary Fig. 5**)[25]. Comparing the profiles for M2BP and whole serum (**Fig. 2b**), we quickly identified 6 lectins with a high S/N ratio. Interestingly, all lectins identifying fucose modification, which is the most well-known glyco-alteration in liver disease (*Pisum sativum* agglutinin (PSA), *Lens culinaris* agglutinin (LCA), *Aspergillus oryzae* lectin (AOL), and *Aleuria aurantia* lectin (AAL)), were high-noise lectins (**Fig. 2b**). After subtraction, we used both the Mann–Whitney *U* test as a nonparametric test, and receiver-operating characteristic (ROC) analysis, to characterize the diagnostic accuracy of the candidate lectins at each stage of fibrosis: significant fibrosis (F2/F3/F4), severe fibrosis (F3/F4) and cirrhosis (F4) (**step 3**). As a result, we found that the diagnostic score of *Wisteria floribunda* agglutinin (WFA) was superior to the other 5 lectins at every fibrosis stage (**Fig. 2c and Supplementary Fig. 6**).

"Proof-of-concept" experiment for direct quantitation of the serum WFA-binding M2BP by sandwich immunoassay. We quantitatively analyzed the WFA-binding M2BPs (WFA^+-M2BP) in serum. Sera, pretreated as described in the **Methods**, were firstly subjected to affinity capture with 20 μl slurry of WFA-coated agarose gel. The eluted fraction was immunoprecipitated with a capturing antibody against M2BP and the product was analyzed by Western blot. The intensity of the "smearing-band" signal for WFA^+-M2BP gradually increased in proportion to the severity of liver fibrosis (**Supplementary Fig. 7**), as indicated by the red line shown in

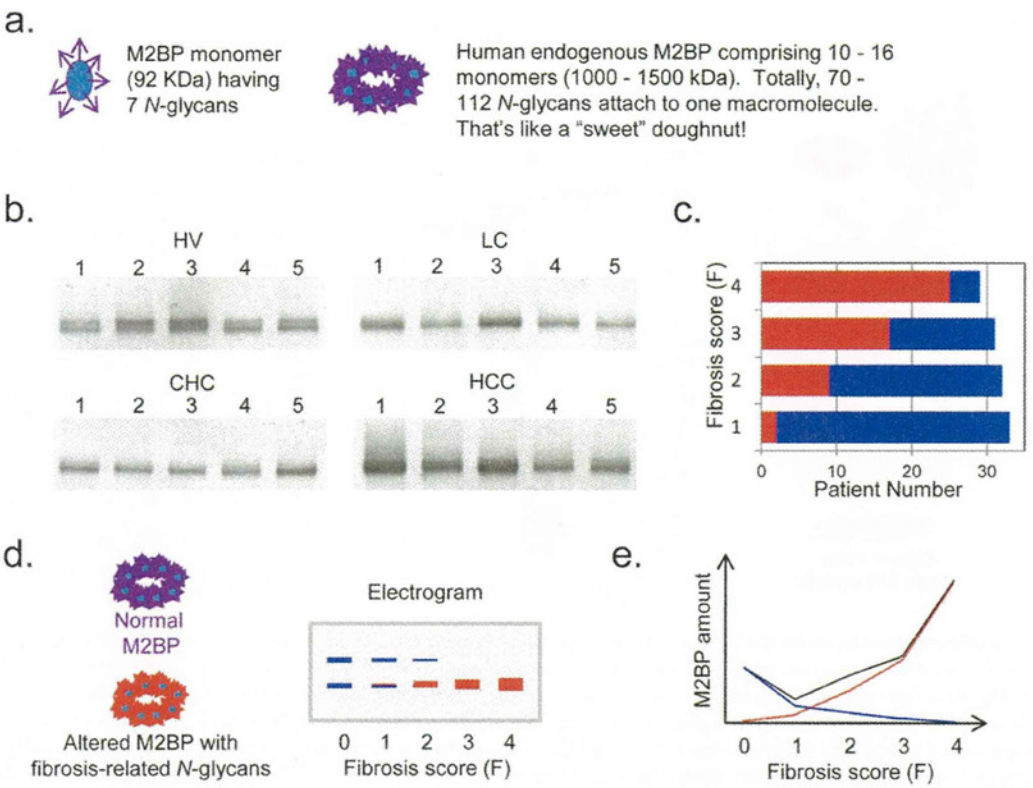

Figure 1 | Changes in the quality and quantity of human serum M2BP with progression of liver fibrosis. (a) The unique shape of human endogenous serum M2BP. The arrowheads and circles represent the *N*-glycan moieties and core protein respectively. (b) Western blot analysis: M2BPs in 2 μl of serum were purified by immunoprecipitation before SDS-PAGE. HV, healthy volunteer; CHC, patient with chronic hepatitis C; LC, HCV-infected patient with liver cirrhosis; and HCC, HCV-infected patient with hepatocellular carcinoma. (c) Number of patients with single (red) or double (blue) band appearance on the blot. The number of bands was determined visually by two independent analysts. The total number of HCV patients who participated in this study was 125 (F0–F1 [$n = 33$], F2 [$n = 32$], F3 [$n = 31$], and F4 [$n = 29$]). (d) Typical changes of serum M2BP band intensities in patients with different fibrosis scores and (e) concentrations based on a previous report on quantitation of serum M2BP by Cheung *et al*[3]. and our present results. The blue bands on the electrogram and blue line on the graph represent M2BPs secreted from normal liver. The red bands and line represent altered M2BP, the concentration of which is suggested to increase with the progression of fibrosis. The black line represents the total concentration of serum M2BP.

Fig. 1e. We next conducted a sandwich immunoassay with WFA and anti-M2BP antibody (see **Supplementary Fig. 3b**). WFA was immobilized on the surface of a 96-well microtiter plate through biotin–streptavidin interaction. We performed the first assay for the WFA-binding activity using recombinant human M2BP (rhM2BP). As a result, a linear regression analysis revealed a linear range of detection from 0.039 to 0.625 μg/ml (**Supplementary Fig. 8a**). Subsequently, we used culture supernatant of a hepatoblastoma cell line HepG2, which expresses WFA^+-M2BP, to illustrate the dose-dependency of the interaction of WFA with M2BP/HepG2. We also showed that heat treatment of the culture supernatant eliminated this binding activity (**Supplementary Fig. 8b**). Finally, we performed a sandwich immunoassay for direct measurement of WFA^+-M2BP in untreated serum samples, and the results correlated well with the quantitative assay using affinity capture and lectin microarray analysis (**Supplementary Fig. 7 and 9**).

FastLec-Hepa: a fully automated sandwich immunoassay for direct quantitation of serum WFA^+-M2BP. We adapted the WFA-antibody immunoassay to the HISCL-2000i bedside clinical chemistry analyzer[18]. We successfully adjusted every reaction condition during the automatic assay by HISCL, which is about a 17-min manipulation. Heat pretreatment of the serum was avoided to ensure both binding avidity and the fast association rate. Repeatability was assessed by performing 10 independent assays of three samples, and the coefficient of variation ranged between 2.1% and 2.5% (data not shown). Sensitivity was determined by triplicate assays of samples generated by 2-fold serial dilution of 50 μg/ml rhM2BP. The linear regression analysis identified a linear range of detection ($R^2 = 1.00$) from 0.025 to 12.5 μg/ml (**Fig. 3a,** a range of 0.025 to 1.6 μg/ml also shown in **Fig. 3b**). The resulting dynamic range was 25-fold that of the manual sandwich immunoassay described above. We next examined whether the HISCL measurements made on serum from HCV patients ($n = 125$) were consistent with lectin microarray analysis, and this comparison resulted in sufficient linearity with coefficient of determination, $R^2 = 0.848$ (**Fig. 3c**). Accordingly, we could perform automatic quantitation of serum WFA^+-M2BP in 180 patients in 1 hour and we have therefore named it FastLec-Hepa.

Validation of FastLec-Hepa. For a validation study, we obtained serum from CH patients at two locations: Nagoya City University Hospital and Hokkaido University Hospital (**Supplementary Fig. 10**). Staging of these patients ($n = 209$) by histological activity index (HAI) was conducted independently by two senior pathologists on ultrasonography-guided liver biopsy samples. F0–F1 was assigned in 82 cases (39.2%), F2 in 52 (24.9%), F3 in 40 (19.1%), and F4 (cirrhosis) in 35 (16.7%). Serum from healthy volunteers (with no history of any hepatitis virus infections) was obtained for analysis from two sites ($n = 48$ from National Institute of Advanced Industrial Science and Technology [AIST]: HV1; $n = 70$ from Nagoya City University: HV2). Their FastLec-Hepa counts

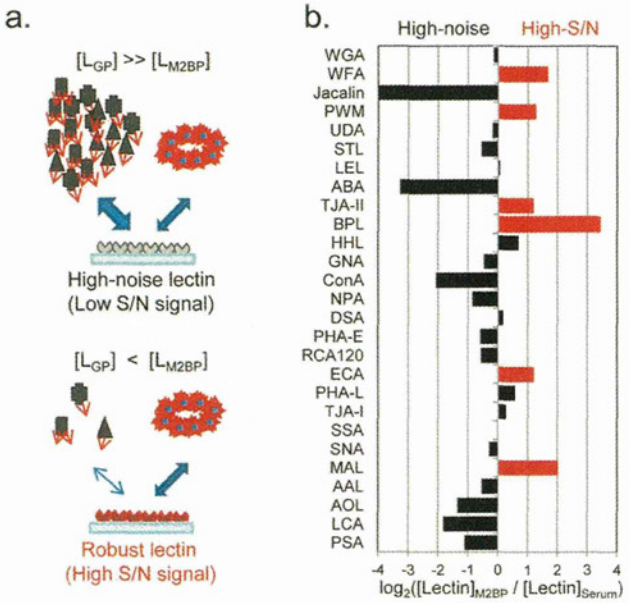

c.

	MAL	ECA	BPL	TJAII	PWM	WFA
1) Cirrhosis						
AUC	0.69	0.89	0.9	0.88	0.85	0.9
Sensitivity (%)	90	72	79	93	79	93
Specificity (%)	49	88	85	71	83	76
P-value	2.2×10^{-3}	3.2×10^{-10}	6.2×10^{-11}	5.1×10^{-10}	7.5×10^{-9}	5.5×10^{-11}
2) Severe fibrosis						
AUC	0.72	0.8	0.82	0.81	0.78	0.85
Sensitivity (%)	68	83	80	77	75	70
Specificity (%)	74	77	75	82	77	85
P-value	2.8×10^{-5}	6.2×10^{-9}	1.0×10^{-9}	2.0×10^{-9}	8.8×10^{-8}	3.0×10^{-11}
3) Significant fibrosis						
AUC	0.64	0.69	0.75	0.74	0.67	0.78
Sensitivity (%)	82	66	64	57	60	89
Specificity (%)	48	76	85	88	82	61
P-value	1.7×10^{-2}	1.3×10^{-3}	1.7×10^{-5}	4.6×10^{-5}	3.3×10^{-3}	1.3×10^{-6}

Figure 2 | Selection of the optimal lectin for the lectin-antibody sandwich immunoassay. (a) The kinetics of lectins binding to serum glycoproteins. The M2BP-binding lectins are divided into two categories: high-noise lectins and high signal-to-noise (S/N) lectins. The high-noise lectins bind to both M2BPs and abundant serum glycoproteins, causing a strong suppression of the M2BP–lectin interaction (see *top panel*). On the other hand, the number of binding targets in serum for the high S/N lectins is negligible, resulting in the specific interaction with the target M2BP (see *lower panel*). (b) Classification of M2BP-binding lectins. The high S/N lectins are those detecting M2BPs with at least twice the signal intensity seen for other serum glycoproteins. The classification strategy is summarized in **Supplementary Fig. 4**. (c) Diagnostic performance of 6 candidate lectins. *P*-values were determined using the nonparametric Mann–Whitney *U* test (Excel 2007, Microsoft).

(**Supplementary Table 1**) are also plotted in a box-whisker diagram in **Supplementary Fig. 11** along with that from a separate group of 1,000 healthy volunteers (HV3). Based on the calibration curve ([FastLec-Hepa counts]/10^6 = 1.027 × [rhM2BP] + 0.006 in **Fig. 3a, b**), the 75th percentiles of HVs of 64,205–107,617 and the 25th percentile of LC of 1,327,596 patients (see also **Supplementary Fig. 11**), we estimate the concentration of WFA$^+$-M2BP to be approximately 0.09 μg/ml in the serum of HV patients and > 1.0 μg/ml in that of LC patients. This means that the linear range shown in **Fig. 3a** is sufficient for accurate quantitation of WFA$^+$-M2BP in all serum samples. The analyses showed a gradual increase with the progression of liver fibrosis, but it did not correlate with the grade of hepatic activity defined by HAI scoring (**Supplementary Fig. 12**).

Next, we made a statistical comparison of FastLec-Hepa with other simple tests for liver fibrosis: the direct fibrosis marker hyaluronic acid (HA), the indirect fibrosis index FIB-4[26] and the glycan-based fibrosis index LecT-Hepa[18,27]. We enrolled 160 patients (F0−F1 = 66, F2 = 41, F3 = 33 and F4 = 20) whose age, platelet count, AST, ALT and HA levels were readily available (**Supplementary Fig. 10** and **Supplementary Tables 1 and 2**). As shown in **Fig. 4a**, the results of all the tests correlated well with the stage of fibrosis ($P < 0.0001$). However, an ROC analysis concluded that FastLec-Hepa detected cirrhosis with the highest diagnostic accuracy (**Fig. 4b** and **Table 1**). Notably, FastLec-Hepa distinguished between F3 and F4 with 90% sensitivity, 85% specificity, and with an AUC of 0.91. These results were superior to LecT-Hepa (sensitivity:

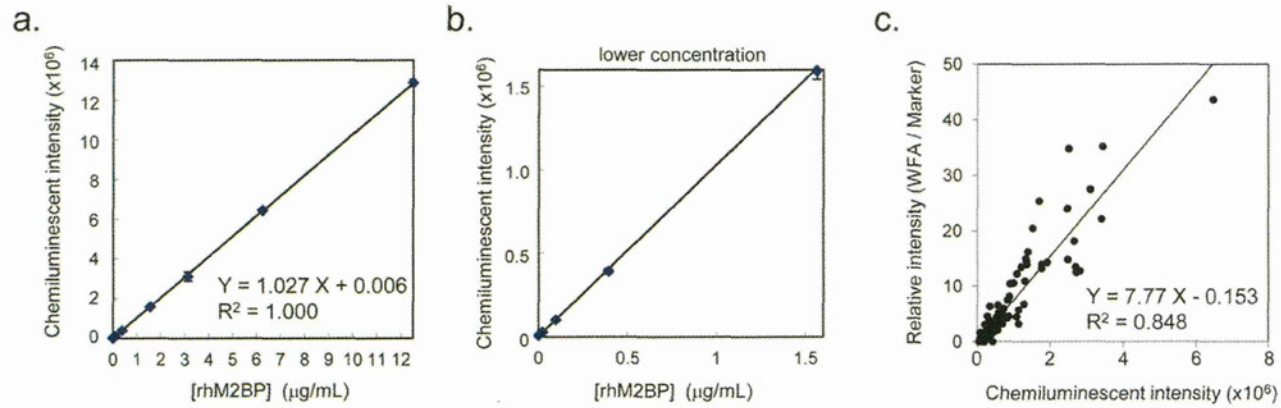

Figure 3 | Description of FastLec-Hepa, a fully automated WFA and anti-M2BP antibody sandwich immunoassay. (a) Standard curve for quantitation of WFA-binding rhM2BP. Plots for the lower concentration of rhM2BP are alternatively highlighted in (b). (c) Scatterplot comparison of WFA$^+$-M2BP data obtained from 125 different serum samples by both HISCL and a manual lectin microarray assay. The best-fit linear comparison with its correlation coefficient was calculated in Excel 2007 (Microsoft).

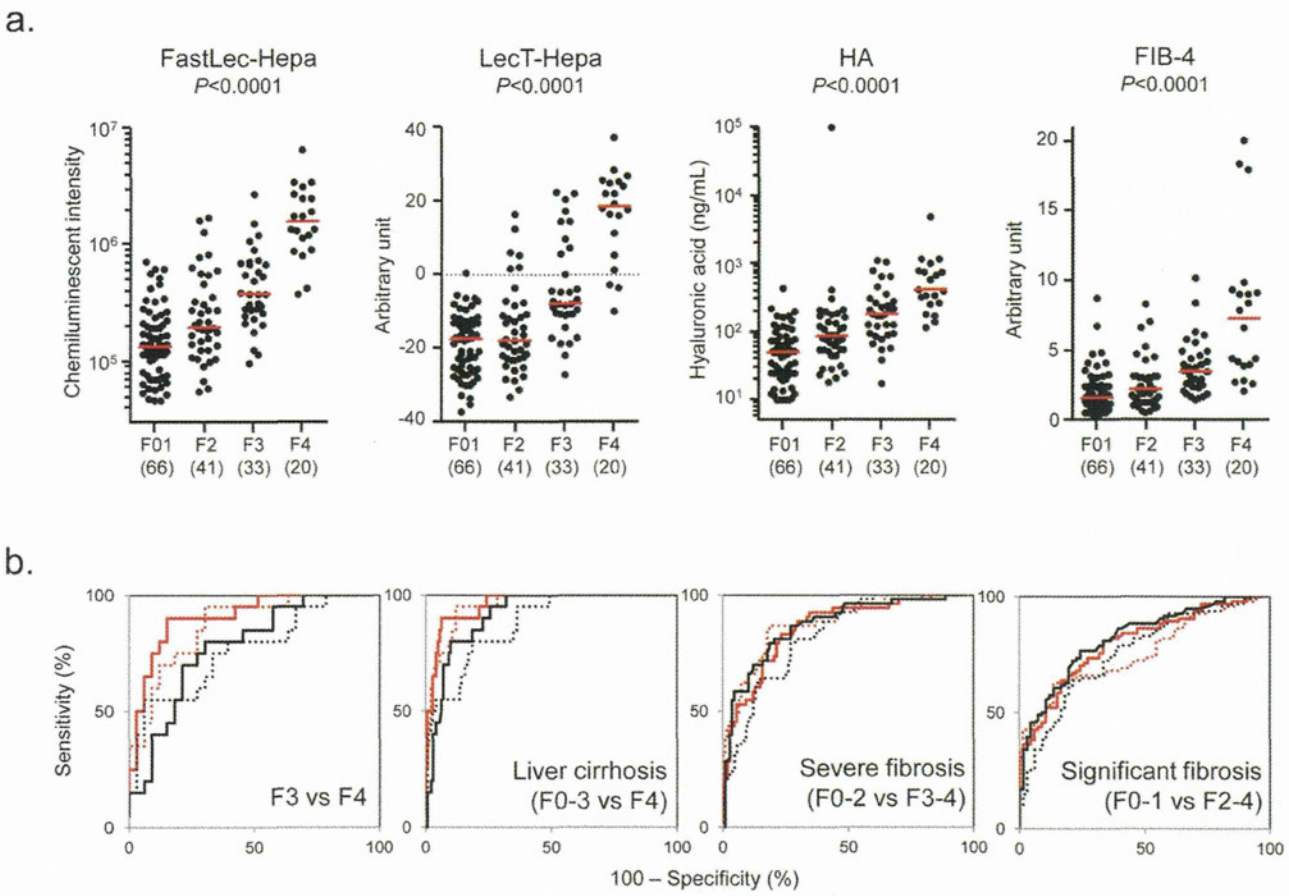

Figure 4 | Comparison of diagnostic performance of FastLec-Hepa, LecT-Hepa, HA, and FIB-4. (a) Scatterplots of the data obtained with FastLec-Hepa, LecT-Hepa, HA, and FIB-4 against the fibrosis score. Red horizontal lines represent the median. Correlation of the data with the progression of fibrosis was evaluated as significant differences in the medians relative to the fibrosis scores ($P < 0.0001$) by a nonparametric method, the Kruskal–Wallis one-way ANOVA. (b) Area under the receiver-operating characteristic (AUC-ROCs) curves of FastLec-Hepa, LecT-Hepa, HA, and FIB-4 for liver cirrhosis (F3 vs F4 or F0–3 vs F4), severe fibrosis (F0–2 vs F3–4), and significant fibrosis (F0–1 vs F2–4). FastLec-Hepa, LecT-Hepa, HA, and FIB-4 are indicated by a red solid line, red dotted line, black solid line, and black dotted line, respectively.

95%, specificity: 70%, and AUC: 0.87), FIB-4 (sensitivity: 55%, specificity: 94%, and AUC: 0.76), and HA (sensitivity: 80%, specificity: 70%, and AUC: 0.78).

Clinical utility of FastLec-Hepa: quantitative monitoring of antiviral therapy. To assess clinical utility, we examined two types of trials—short-interval evaluation and long-term follow-up—both of which are essential for following the patients receiving PEG-interferon-α and ribavirin therapy. For the first trial, we enrolled 41 patients with CHC who had previously undergone 48 weeks of therapy at Hokkaido University Hospital. According to the definition described in the **Methods**, 26 and 15 of them were judged as SVR and NVR/relapse (non-SVR), respectively. For each patient, we performed FastLec-Hepa on serum samples, which were collected just before treatment (Pre) and within a short period (12–22 weeks) after treatment (Post) (**Fig. 5a**). We found a marked decrease from Pre to Post counts ($P = 0.0061$) in SVR patients, but no apparent change for non-SVR patients ($P = 0.9780$) (**Fig. 5b**). Specifically, a median percent decrease of 31% was found for SVR patients (median Pre-count of 161,053 and median Post-count of 110,739), while the level for non-SVR patients was essentially constant. These results show that the assay can evaluate the effect of therapy within a short period after treatment. This is an important advance, because the ALT levels of non-SVR, as well as SVR, are mostly decreased into the range of 10–64 IU/ml during this period (**Fig. 5c**)[5]. In fact, changes in the FastLec-Hepa counts did not correlate with those in the ALT counts (**Supplementary Fig. 13**), thereby invalidating ALT-dependent fibrosis assays, including FIB-4 (**Fig. 5d**).

In support of our finding that the FastLec-Hepa counts correlate excellently with the stage of fibrosis, we found a strong correlation between the histopathological scores and the median of the $\log_{10}$[FastLec-Hepa] counts (**Fig. 5e**). These correlations were approximated to two linear equations: $y = 0.23x + 4.9$ for F0 to F3, and $y = 0.58x + 3.8$ for F3 to F4 histology. This means that FastLec-Hepa can reliably reproduce the assessment of therapeutic effects, which were previously drawn from histopathological scoring[9]. Indeed, the median changes in fibrosis obtained by FastLec-Hepa analysis were about −0.295 stages/year for SVR and 0.010 stages/year for non-SVR (**Fig. 5f**). These data were consistent with the rate of fibrosis progression and regression determined by Shiratori *et al*[9].

For the second trial, we enrolled 6 HCV patients (SVR = 3 and non-SVR = 3) with advanced fibrosis who completed 48 weeks of therapy at Nagoya City University Hospital. Sera were collected before therapy and at 0, 1, 3, and 5 years after the end of therapy (see **Fig. 5g**). FastLec-Hepa counts in SVR patients gradually decreased and reached below the median of F0 patients within 3 years. However, those in non-SVR patients remained above the median for F3 patients during the follow-up period (**Fig. 5h**).

Table 1 | Diagnostic performance of fibrosis markers

$n = 160$	FIB-4	HA	LecT-Hepa	FastLec-Hepa
a) Significant fibrosis (F0–1 vs F2–4)				
AUC	0.76	0.82	0.76	0.79
(95% CI)	(0.68–0.83)	(0.76–0.89)	(0.69–0.83)	(0.72–0.86)
Diagnostic sensitivity (%)	64	77	63	81
Diagnostic specificity (%)	79	76	86	67
Youden's index (%)	43	52	49	48
b) Severe fibrosis (F0–2 vs F3–4)				
AUC	0.83	0.87	0.88	0.84
(95% CI)	(0.76–0.89)	(0.81–0.93)	(0.82–0.93)	(0.77–0.91)
Diagnostic sensitivity (%)	81	81	87	83
Diagnostic specificity (%)	71	79	81	77
Youden's index (%)	52	61	68	60
c) Liver cirrhosis (F0–3 vs F4)				
AUC	0.88	0.91	0.95	0.96
(95% CI)	(0.80–0.95)	(0.86–0.96)	(0.92–0.99)	(0.93–0.99)
Diagnostic sensitivity (%)	80	80	95	90
Diagnostic specificity (%)	81	90	88	94
Youden's index (%)	61	70	83	84
d) Liver cirrhosis (F3 vs F4)				
AUC	0.76	0.78	0.87	0.91
(95% CI)	(0.63–0.90)	(0.65–0.90)	(0.77–0.97)	(0.82–0.99)
Diagnostic sensitivity (%)	55	80	95	90
Diagnostic specificity (%)	94	70	70	85
Youden's index (%)	49	50	65	75

Interestingly, HCC had developed in two non-SVR patients whose FastLec-Hepa counts remained above the median of F4 patients throughout. Other fibrosis indices, such as FIB-4 and biochemical parameters (ALT and AST), did not distinguish between SVR and non-SVR or appear to predict this occurrence (**Fig. 5i-k**).

Discussion

We have described the development and use of a fully automated, glycan-based immunoassay termed FastLec-Hepa, for the evaluation of liver fibrosis. A high degree of reliability in the quantitative aspects of this method should establish it as a clinically significant test,

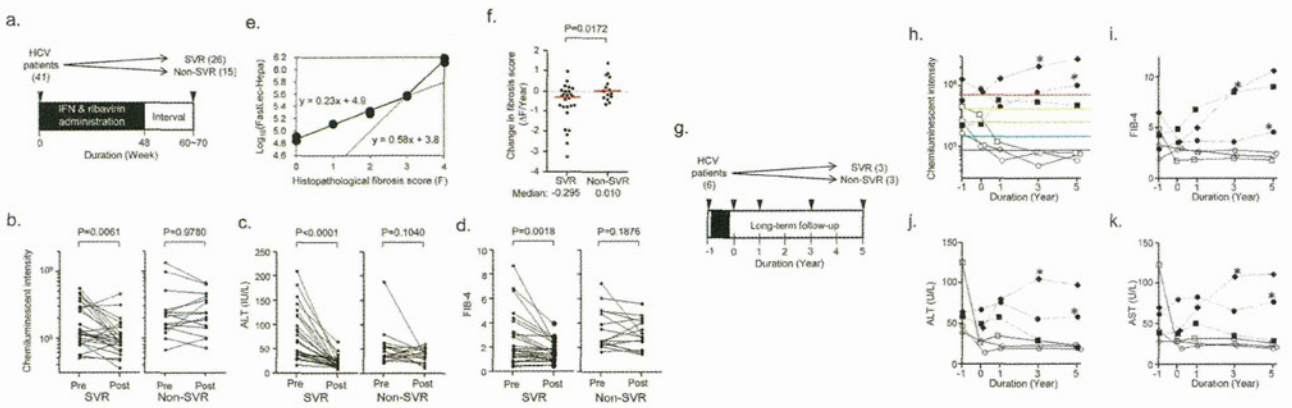

Figure 5 | Evaluation of the curative effect of interferon therapy by FastLec-Hepa. (a) Validation of FastLec-Hepa in short-interval evaluation. The numbers in parentheses represent the number of patients participated in this experiment. Arrowheads indicate the timing of blood collection. At week 0, blood was collected immediately before the treatment. Black box indicates the period of PEG-interferon-α and ribavirin therapy. Changes in the FastLec-Hepa counts (b), ALT (c), and the FIB-4 index (d) in patients with sustained virologic response (SVR) and relapse/nonresponders (non-SVR) during interferon therapy. The *P*-value was determined by a nonparametric method, the Wilcoxon matched pairs signed-rank test. (e) Dot-plot representation of the histopathological fibrosis score and the medians of FastLec-Hepa counts. Best-fit linear curves were calculated in Excel 2007 (Microsoft) allowing conversion of the FastLec-Hepa counts into fibrosis score. (f) Yearly changes in the converted fibrosis score. Changes for patients with SVR and non-SVR are indicated in the dot plots. Red horizontal lines represent the median. The *P*-value was determined by the Mann–Whitney *U* test. (g) Validation of FastLec-Hepa in long-term follow-up. The numbers in parentheses represent the number of patients participated in this experiment. Arrowheads indicate the timing of blood collection. At year -1 and 0, the blood was collected immediately before and after the treatment, respectively. Black box indicates the period of PEG-interferon-α and ribavirin therapy. Yearly changes of FastLec-Hepa counts (h), FIB-4 index (i), ALT (j), and AST (k) in individual patients after therapy. The five colored lines in (h) represent the median values obtained for each fibrosis stage (red, F4; orange, F3; green, F2; cyan, F1; blue, F0). Closed and opened symbols indicate the data obtained from non-SVR and SVR patients, respectively. * indicates the period when the development of HCC was found.

particularly for revealing and managing patients at a high risk of progression to liver complications such as HCC and related life-threatening events. The most striking advantage of FastLec-Hepa is not only its simplicity but also its capacity to provide fibrosis readouts that are not influenced by fluctuations in the ALT value or inflammation, both of which can cause falsely high estimates in most of the other fibrosis tests available[10]. In fact, our study has illustrated robust capacity of FastLec-Hepa to evaluate the effects of antiviral therapy and subsequent disease progression in both the short and long term.

Many retrospective and prospective studies have demonstrated that achieving SVR through the PEG-interferon-α/ribavirin treatment significantly reduces liver-related morbidity and mortality (i.e., hepatic decompensation, HCC, and liver-related death)[28–30]. As this combination therapy is effective in only about 50% of patients with HCV genotype 1, new agents[1] and targets[31] for antiviral treatments of HCV have been developed to achieve SVR more effectively after the therapy. Long-term follow-ups often show that the risk of disease progression is significantly high in patients with non-SVR after PEG-interferon-α/ribavirin treatment. Furthermore, the development of HCC in patients with SVR remains at a significant cumulative rate (2%)[28,30,32,33]. For these reasons, a new data-mining model using individual factors (age, platelet count, serum albumin and AST) was developed recently to identify patients at a high risk of HCC development[34]. This is, however, a statistical procedure for estimating the chance of disease progression, and there is not a direct evaluation of fibrosis. In the present report, we performed a long-term retrospective study with serially collected sera from SVR and non-SVR patients, in which we showed the potential use of FastLec-Hepa for improved prognostic accuracy. Indeed, recent advances in the development of antifibrotic agents lead us to expect the therapeutic elimination of health risks associated with HCC and decompensation[35]. Moreover, we expect that FastLec-Hepa will be proved for its usefulness in rapid evaluation of progression and regression of fibrosis in clinical trials of newly developed antifibrotic agents. Hence, FastLec-Hepa should be very useful for fibrosis stage screening and evaluation of disease progression in untreated individuals or patients under or after treatment, as well as evaluation of the most recently developed drugs.

It is important to note that FastLec-Hepa has many merits, including speed (possibly 1,000 assays per day) and full automation for measurement of a serological glycobiomarker: these attributes will enable retrospective studies with valuable serum specimens that have been collected previously. In addition, our recently developed calibrator for FastLec-Hepa will improve traceability and enable simultaneous assay and data storage in multiple diagnostic facilities. The data obtained with diluted serum samples demonstrated a high level of assay reproducibility and a very favorable linear detection range (**Supplementary Fig. 14**). Furthermore, we found an excellent agreement between assay values for serum and plasma prepared simultaneously from the same patient. Presently, we have about 10,000 sera and plasma available with detailed clinical notes collected in more than 10 facilities in Japan, and a series of retrospective studies is under way. We will shortly conclude licensing of our system for clinical implementation, based largely on the trials of the present study. In contrast to this, the majority of recent noninvasive techniques are currently shifting to physical measurements such as FibroScan, acoustic radiation force impulse[36] and real-time strain elastography[37]. Any on-site assay of large numbers of blood samples should provide a diagnostic value comparable to that of FibroTest, and a direct comparison in the same patient group will be necessary to evaluate this. We note here that according to a recent statistical validation method[38], predicted AUC of the diagnostic value of FibroTest for detection of advanced fibrosis in our sample set (DANA score = 1.81) was approximately 0.77, which was comparable to the AUC of FastLec-Hepa we obtained (0.79).

FastLec-Hepa has adopted a new paradigm for clinical diagnosis, "glyco-diagnosis", which is based on the quantity and quality of protein glycosylation patterns that well indicate disease progression. To detect such changes in glycosylation by conventional methods (e.g., mass spectrometry, liquid chromatography, or capillary electrophoresis), it is absolutely necessary to liberate the glycans of interest from their protein linkages[15,17,39]. It is possible to employ an alternative technology, which is based on a lectin–antibody sandwich immunodetection system for intact glycoproteins bearing disease-specific glyco-alterations. Such assays have been used to detect changes in fucosylation of *N*-linked glycans, which are associated with liver disease. However, in the present study, fucose-binding lectins were classified as "high noise" (**Fig. 2b**), and thus an enrichment of the target protein was the essential process in the assay. Lectin-overlay detection is performed typically after on-plate enrichment of the target glycoproteins by an immobilized antibody. In such cases, detection relies on a low avidity (high dissociation rate) between the captured glycoprotein and the overlaid lectin probe (see *right* of **Supplementary Fig. 3b**). These kinetic considerations essentially eliminate the use of an automated bedside clinical chemistry analyzer. Even though a fucose-binding lectin was immobilized on the beads (see *left* of **Supplementary Fig. 3b**), it still remains a problem for reliable quantitation by autoanalyzer. Our previous system LecT-Hepa[16,18,19,26], which detects the level of fucosylated α1-acid glycoprotein, requires enrichment of the protein prior to the assay.

In the present study, we have developed a strategy to overcome these problems in glyco-diagnosis associated with clinical implementation, and realized a rapid "on-site diagnosis" system (17 min, within the minimum time required for single assay by HISCL), based on analysis of a glycomarker (**Supplementary Fig. 1**). The strategy for selecting the most robust lectin led us to WFA, and away from the use of fucose-binding lectins, for the direct measurement system (**Fig. 2**). The diagnostic utility of M2BP, a protein resembling "sweet-doughnut"[20], brought a favorable density and orientation of the disease-related glycan on the homomultimer. These characteristic structures resulted in a major increase in the avidity of M2BP for the plated WFA. The resulting glycan–lectin interaction, which is remarkably strong and specific, made it possible to develop the rapid and highly sensitive assay (see *left* of **Supplementary Fig. 3b**). We believe that this unique strategy will revolutionize the use of glyco-diagnosis in clinical medicine and potentially provide a framework for the development of a new generation of biomarker assays.

Methods

Patient samples, biochemical parameters and indices. Patients with chronic hepatitis were enrolled at Nagoya City University Hospital and Hokkaido University Hospital. Healthy volunteers as the controls were randomly selected in Nagoya City University Hospital (70 individuals) and AIST (48 individuals). The institutional ethics committees at Nagoya City University Hospital, Hokkaido University Hospital, and AIST approved this study, and informed consent for the use of their clinical specimens was obtained from all participants before the collection. In addition, we used 1,000 serum samples from virus-negative Caucasians as the normal population, which were purchased from Complex Antibodies Inc. (Fort Lauderdale, FL) and collected under IRB-approved collection protocols. Fibrosis was graded in the patients according to the histological activity index (HAI) using biopsy or surgical specimens. Biopsy specimens were classified as follows: F0, no fibrosis; F1, portal fibrosis without septa; F2, few septa; F3, numerous septa without cirrhosis; and F4, cirrhosis. The three diagnostic targets in this study were defined as significant fibrosis: F2+F3+F4; severe fibrosis: F3+F4; and cirrhosis: F4. Hepatic inflammation was also assessed according to the HAI, as follows: A0, no activity; A1, mild activity; A2, moderate activity; and A3, severe activity. Cirrhosis was confirmed by ultrasonography (coarse liver architecture, nodular liver surface, and blunt liver edges), evidence of hypersplenism (splenomegaly on ultrasonography) and/or a platelet count of $< 100{,}000/mm^3$. Virological responses during PEG-interferon-α and ribavirin therapy were defined as follows[5]: SVR, absence of HCV RNA from serum 24 weeks following discontinuation of therapy; nonresponder, failure to clear HCV RNA from serum after 24 weeks of therapy; relapse, reappearance of HCV RNA in serum after therapy was discontinued. For all patients, age and sex were recorded and serum levels of the following were analyzed: aspartate aminotransferase (AST), alanine aminotransferase (ALT), γ-glutamyltransferase (GGT), total bilirubin,

albumin, cholinesterase, total cholesterol, platelet count (PLT), hyaluronic acid (HA). The FIB-4 index was calculated as follows: [age (years) × AST (U/L)]/[platelets (10^9/L) × ALT (U/L)$^{1/2}$][26]. Fibrosis-specific glyco-alteration of α1-acid glycoprotein was determined by lectin–antibody sandwich immunoassays with a combination of three lectins (*Datura stramonium* agglutinin (DSA), *Maackia amurensis* leukoagglutinin (MAL), and *Aspergillus oryzae* lectin (AOL))[16]. All assays used an automated chemiluminescence enzyme immunoassay system (HISCL-2000i; Sysmex Co., Kobe, Japan)[18].

Enrichment of M2BP from serum. An automated protein purification system (ED-01; GP BioSciences Ltd., Yokohama, Japan) was used to immunoprecipitate M2BP from serum specimens. In brief, sera (2 μl) were diluted 10-fold with PBS/0.2%(w/v) SDS, heated at 95°C for 20 min, mixed with 10 μl of Triton X-100 in TBS (TBSTx) and injected into a 96-well SUMILON microtiter plate (Sumitomo Bakelite Co., Ltd., Tokyo, Japan). The plate and working reagents, including biotinylated anti-M2BP antibody (10 ng/μl), streptavidin-coated magnetic beads, washing buffer (1% TBSTx) and elution buffer (TBS containing 0.2% SDS), were loaded into the system. This generated 110 μl of purified M2BPs per serum sample (96 samples in 3.5 h).

Western blot analysis. Anti-human M2BP polyclonal antibody was purchased from R&D Systems, Inc. (Minneapolis, MN) and biotinylated with Biotin Labeling Kit – NH_2 (Dojindo Laboratories, Kumamoto, Japan). Purified serum M2BPs were electrophoresed under reducing conditions on 5–20% polyacrylamide gels (DRC, Tokyo, Japan) and transferred to PVDF membranes. After treatment with Block Ace® (DS Pharma Biomedical Co., Ltd., Osaka, Japan), the membranes were incubated with biotinylated anti-M2BP polyclonal antibody, and then with alkaline phosphatase-conjugated streptavidin (1/5000 diluted with TBST; ProZyme, Inc., San Leandro, CA). The membranes were incubated with Western Blue stabilized substrate for alkaline phosphatase (Promega, Madison, WI).

Lectin microarray analysis. Enriched M2BPs were analyzed with an antibody-overlay lectin microarray[24]. Purified protein (14 μl) was diluted to 60 μl with PBS containing 1%(v/v) Triton X-100 (PBSTx); this was applied to a LecChip™ (GP BioSciences Ltd.), which included three spots of 45 lectins in each of seven reaction wells. After incubation for 12 h at 20°C, 2 μl of human serum IgG (10 mg/ml) was added to the reaction solution on each chip and incubated for 30 min. The reaction solution was then discarded, and the chip was washed three times with PBSTx. Subsequently, 60 μl (200 ng) of biotinylated anti-human M2BP in PBSTx was applied to the chip, and incubated for 1 h. After three washes with PBSTx, 60 μl (400 ng) of a Cy3-labeled streptavidin (GE Healthcare, Buckinghamshire, UK) solution in PBSTx was added and incubated for 30 min. The chip was rinsed with PBSTx, scanned with an evanescent-field fluorescence scanner (GlycoStation™ Reader1200; GP BioSciences Ltd.) and analyzed with the Array Pro Analyzer software package, version 4.5 (Media Cybernetics, Inc., Bethesda, MD). The chip was scanned with the gain set to register a maximum net intensity < 40,000 for the most intense spots. The net intensity value for each spot was calculated by subtracting the background value from the signal intensity value. The relative intensity of lectin-positive samples was determined from the ratio of their fluorescence to the fluorescence of the internal-standard lectin, DSA.

Quantitation of *Wisteria floribunda* agglutinin (WFA)-binding M2BP. Serum was pretreated as described above under enrichment of M2BP from serum. Pretreated samples (50 μl) were diluted with an equal volume of starting buffer (0.1%(w/v) SDS in PBSTx), added to the WFA-coated agarose in a microtube (20 μl slurry; Vector Lab., Burlingame, UK), and incubated at 4°C for 5 h with gentle shaking. After centrifugation of the reaction solution at 2000 × *g* for 10 min, the supernatant was removed to a new microtube. The precipitate was suspended in 50 μl of the starting buffer, recentrifuged and this second supernatant combined with the first (designated as path-through fraction T). The precipitate was then washed with 200 μl of the starting buffer and the bound glycoproteins were eluted with 60 μl of 200 mM galactosamine/0.02%(w/v) SDS in PBS (designated as elution fraction E). M2BP was immunoprecipitated from fractions T and E and examined by electrophoresis under reducing conditions on 5–20% gradient SDS–polyacrylamide gels.

WFA-antibody sandwich ELISA. Flat-bottomed 96-well streptavidin-precoated microtiter plates (Nunc, Int., Tokyo, Japan) were treated with biotinylated WFA (Vector, 250 ng/well) for 1 h at room temperature. The plates were incubated with the diluted serum samples (50 μl) in PBS containing 0.1%(v/v) Tween20 (PBS-t) for 2 h at room temperature and then with 50 ng/well of the anti-human M2BP polyclonal antibody, in PBS-t for 2 h at room temperature. The plates were washed extensively and then incubated with 50 μl of horseradish peroxidase (HRP)-conjugated anti-mouse IgG (Jackson ImmunoResearch Laboratories Inc., Philadelphia, PA) at 1:10,000 in PBS-t for 1 h at room temperature. The substrate 3,3′,5,5′-tetramethylbenzidine (Thermo Fisher Scientific, Fremont, CA) solution (100 μl) was added to each well. The enzyme reaction was stopped by adding 100 μl of 1 M sulfuric acid, and the optical density measured at 450 nm.

WFA-antibody sandwich immunoassay by HISCL. The fibrosis-specific form of glycosylated M2BP was measured based on a sandwich immunoassay approach. Glycosylated M2BP was captured by WFA immobilized on magnetic beads, and the bound product was assayed with an anti-human M2BP monoclonal antibody linked to alkaline phosphatase (ALP-αM2BP). Two reagent packs (M2BP-WFA detection pack and a chemiluminescence substrate pack) were loaded in the HISCL. The detection pack comprised three reagents: a reaction buffer solution (R1), a WFA-coated magnetic beads solution (R2) and an ALP-αM2BP solution (R3). The chemiluminescence substrate reagent pack contained a CDP-Star substrate solution (R4) and a stopping solution (R5). Typically, serum (10 μl) was diluted to 60 μl with R1 and then mixed with R2 (30 μl). After the binding reaction, R3 (100 μl) was added to the reaction solution. The resultant conjugates were magnetically separated from unbound components, and mixed well with R4 (50 μl) and R5 (100 μl) before reading of the fluorescence. The chemiluminescent intensity was acquired within a period of 17 min in the operation described above. The reaction chamber was kept at 42°C throughout.

Statistics. Statistical analyses and graph preparation used Dr. SPSS II Windows software (SPSS Co., Tokyo, Japan), GraphPad Prism 5.0 (GraphPad Software Inc., La Jolla, CA), and Windows Excel 2007. This facilitated selection of the optimal lectin for analysis of fibrosis and a comparison of the diagnostic value of other serological fibrosis markers and indices. Because the data distribution for each parameter was non-Gaussian, the *P*-values were determined by nonparametric tests, such as the Mann–Whitney *U* test and Wilcoxon signed-rank test. Correlations with liver fibrosis were estimated as the significance of differences among the staging groups (F0–1, F2, F3, and F4) determined by Kruskal–Wallis nonparametric one-way analysis of variance. To assess classification efficiencies for detecting significant fibrosis, severe fibrosis and cirrhosis, the receiver-operating characteristic (ROC) curve analysis was also carried out to determine the area under the curve (AUC) values. Cutoff values obtained from Youden's index were used to classify patients. Diagnostic accuracy was expressed in terms of specificity, sensitivity and AUC.

1. "Nature Outlook Hepatitis C" edited by Brody, H. *et al. Nature* **474**, S1–S21 (2011).
2. Ge, D. *et al.* Genetic variation in IL28B predicts hepatitis C treatment-induced viral clearance. *Nature* **461**, 399–401 (2009).
3. Suppiah, V. *et al.* IL28B is associated with response to chronic hepatitis C interferon-alpha and ribavirin therapy. *Nat. Genet.* **41**, 1100–1104 (2009).
4. Tanaka, Y. *et al.* Genome-wide association of IL28B with response to pegylated interferon-alpha and ribavirin therapy for chronic hepatitis C. *Nat. Genet.* **41**, 1105–1109 (2009).
5. Ghany, M. G., Strader, D. B., Thomas, D. L. & Seeff, L. B. Diagnosis, management, and treatment of hepatitis C: an update. *Hepatology* **49**, 1335–1374 (2009).
6. Afdhal, N. H. *et al.* hepatitis C pharmacogenetics: state of the art in 2010. *Hepatology* **53**, 336–345 (2011).
7. Peng, C. Y., Chien R. N. & Liaw, Y. N. Hepatitis B virus-related decompensated liver cirrhosis: benefits of antiviral therapy. *J. Hepatol.* **57**, 442–450 (2012).
8. Chang, T. T. *et al.* Long-term entecavir therapy results in the reversal of fibrosis/cirrhosis and continued histological improvement in patients with chronic hepatitis B. *Hepatology* **52**, 886–893 (2010).
9. Shiratori, Y. *et al.* Histologic improvement of fibrosis in patients with hepatitis C who have sustained response to interferon therapy. *Ann. Intern. Med.* **132**, 517–524 (2000).
10. Castera, L. Non-invasive assessment of liver fibrosis in chronic hepatitis C. *Hepatol. Int.* **5**, 625–634 (2011).
11. Imbert-Bismut, F. *et al.* Biochemical markers of liver fibrosis in patients with hepatitis C virus infection: a prospective study. *Lancet* **357**, 1069–1075 (2001).
12. Calès, P. *et al.* A novel panel of blood markers to assess the degree of liver fibrosis. *Hepatology* **42**, 1373–1381 (2005).
13. Castera, L. *et al.* Prospective comparison of two algorithms combining non-invasive methods for staging liver fibrosis. *J. Hepatol.* **52**, 191–198 (2010).
14. Boursier, J. *et al.* Comparison of eight diagnostic algorithm for liver fibrosis in hepatitis C: new algorithms are more precise and entirely noninvasive. *Hepatology* **55**, 58–67 (2012).
15. Callewaert, N. *et al.* Noninvasive diagnosis of liver cirrhosis using DNA sequencer-based total serum protein glycomics. *Nat. Med.* **10**, 429–434 (2004).
16. Kuno, A. *et al.* Multilectin assay for detecting fibrosis-specific glyco-alteration by means of lectin microarray. *Clin. Chem.* **57**, 48–56 (2011).
17. Vanderschaeghe, D. *et al.* High-throughput profiling of the serum N-glycome on capillary electrophoresis microfluidics systems: toward clinical implementation of GlycoHepatoTest. *Anal. Chem.* **82**, 7408–7415 (2010).
18. Kuno, A. *et al.* LecT-Hepa: A triplex lectin-antibody sandwich immunoassay for estimating the progression dynamics of liver fibrosis assisted by a bedside clinical chemistry analyzer and an automated pretreatment machine. *Clin. Chim. Acta* **412**, 1767–1772 (2011).
19. Du, D. *et al.* Comparison of LecT-Hepa and FibroScan for assessment of liver fibrosis in hepatitis B virus infected patients with different ALT levels. *Clin. Chim. Acta* **413**, 1796–1799 (2012).
20. Sasaki, T., Brakebusch, C., Engel, J. & Timpl, R. Mac-2 binding protein is a cell-adhesive protein of the extracellular matrix which self-assembles into ring-like structures and binds beta1 integrins, collagens and fibronectin. *EMBO J.* **17**, 1606–1613 (1998).
21. Iacovazzi, P. A. *et al.* Serum 90K/MAC-2BP glycoprotein in patients with liver cirrhosis and hepatocellular carcinoma: a comparison with alpha-fetoprotein. *Clin. Chem. Lab. Med.* **39**, 961–965 (2001).

22. Artini, M. *et al.* Elevated serum levels of 90K/MAC-2 BP predict unresponsiveness to alpha-interferon therapy in chronic HCV hepatitis patients. *J. Hepatol.* **25**, 212–217 (1996).
23. Cheung, K. J. *et al.* The HCV serum proteome: a search for fibrosis protein markers. *J. Viral. Hepat.* **16**, 418–429 (2009).
24. Kuno, A. *et al.* Focused differential glycan analysis with the platform antibody-assisted lectin profiling for glycan-related biomarker verification. *Mol. Cell. Proteomics* **8**, 99–108 (2008).
25. Kuno, A. *et al.* Evanescent-field fluorescence-assisted lectin microarray: a new strategy for glycan profiling. *Nat. Met.* **2**, 851–856 (2005).
26. Vallet-Pichard, A. *et al.* FIB-4: an inexpensive and accurate marker of fibrosis in HCV infection. Comparison with liver biopsy and fibrotest. *Hepatology* **46**, 32–36 (2007).
27. Ito, K. *et al.* LecT-Hepa, a glyco-marker derived from multiple lectins, as a predictor of liver fibrosis in chronic hepatitis C patients. *Hepatology* **56**, 1448–1456 (2012).
28. Bruno, S. *et al.* Sustained virological response to interferon-α is associated with improved outcome in HCV-related cirrhosis: A retrospective study. *Hepatology* **45**, 579–587 (2007).
29. Cardoso, A.-C. *et al.* Impact of peginterferon and ribavirin therapy on hepatocellular carcinoma: Incidence and survival in hepatitis C patients with advanced fibrosis. *J. Hepatol.* **52**, 652–657 (2010).
30. Morgan, T. R. *et al.* Outcome of sustained virological responders with histologically advanced chronic hepatitis C. *Hepatology* **52**, 833–844 (2010).
31. Lupberger, J. *et al.* EGFR and EphA2 are host factors for hepatitis C virus entry and possible targets for antiviral therapy. *Nat. Med.* **17**, 589–595 (2011).
32. Iwasaki, Y. *et al.* Risk factors for hepatocellular carcinoma in hepatitis C patients with sustained virologic response to interferon therapy. *Liver Int.* **24**, 603–610 (2004).
33. Ikeda, K. *et al.* Anticarcinogenic impact of interferon on patients with chronic hepatitis C: A large-scale long-term study in a single center. *Intervirology* **49**, 82–90 (2006).
34. Kurosaki, M. *et al.* Data mining model using simple and readily available factors could identify patients at high risk for hepatocellular carcinoma in chronic hepatitis C. *J. Hepatol.* **56**, 602–608 (2012).
35. Schuppan, D. & Pinzani, M. Anti-fibrotic therapy: lost in translation? *J. Hepatolol.* **56**, S66–74 (2012).
36. Rizzo, L. *et al.* Comparison of transient elastography and acoustic radiation force impulse for non-invasive staging of liver fibrosis in patients with chronic hepatitis C. *Am. J. Gastroenterol.* **106**, 2112-2120 (2011).
37. Ferraioli, G. *et al.* Performance of real-time sitrain elastography, transient elastgraphy, and aspartate-to-platelet ration index in the assessment of fibrosis in chronic hepatitis C. *AJR Am. J. Roentgenol.* **199**, 19–25 (2012).
38. Poynard, T. *et al.* Standardization of ROC curve areas for diagnostic evaluation of liver fibrosis markers based on prevalences of fibrosis stages. *Clin. Chem.* **53**, 1615–1622 (2007).
39. Nishimura, S. Toward automated glycan analysis. *Adv. Carbohydr. Chem. Biochem.* **65**, 219–271 (2011).

Acknowledgments

This work was supported in part by a grant from New Energy and Industrial Technology Development Organization of Japan. We thank H. Ozaki, H. Shimazaki, S. Unno, K. Saito, M. Sogabe, Y. Kubo, J. Murakami, S. Shirakawa, T. Fukuda (AIST), and H. Naganuma (NCU) for technical assistance. We also thank A. Togayachi, T. Sato, H. Kaji, J. Hirabayashi, H. Tateno, A. Takahashi (AIST) and C. Tsuruno, S. Nagai and Y. Takahama (Sysmex Co.) for critical discussion.

Author contributions:

A.K. conceived and designed the study, performed most of the biochemical experiments, analyzed data and wrote the paper with comments from Y.T., M.M. and H.N.; Y.I. conceived and designed the study, performed the sample pre-treatment for the assay, and analyzed data; Y.T., K.I., M.M., and S.H collected clinical samples, designed the validation study, and analyzed data; A.M. and S.S. performed the biochemical experiments including lectin microarray analysis and analyzed data; M.S. and M.K. performed staging of biopsy specimens by histological activity index (HAI); H.N. conceived and designed the study, and supervised all aspects of the work; and all authors discussed the results and implications, and commented on the paper.

Additional information

Supplementary information accompanies this paper at http://www.nature.com/scientificreports

Competing financial interests: The authors declare no competing financial interests.

How to cite this article: Kuno, A. *et al.* A serum "sweet-doughnut" protein facilitates fibrosis evaluation and therapy assessment in patients with viral hepatitis. *Sci. Rep.* **3**, 1065; DOI:10.1038/srep01065 (2013).

Gut Online First, published on November 7, 2012 as 10.1136/gutjnl-2012-302553

OPEN ACCESS

ORIGINAL ARTICLE

Hepatitis C virus kinetics by administration of pegylated interferon-α in human and chimeric mice carrying human hepatocytes with variants of the *IL28B* gene

Tsunamasa Watanabe,[1] Fuminaka Sugauchi,[2] Yasuhito Tanaka,[1] Kentaro Matsuura,[3] Hiroshi Yatsuhashi,[4] Shuko Murakami,[1] Sayuki Iijima,[1] Etsuko Iio,[3] Masaya Sugiyama,[5] Takashi Shimada,[6] Masakazu Kakuni,[6] Michinori Kohara,[7] Masashi Mizokami[5]

► Additional supplementary files are published online only. To view these files please visit the journal online (http://dx.doi.org/10.1136/gutjnl-2012-302553).

[1]Department of Virology and Liver Unit, Nagoya City University Graduate School of Medical Sciences, Nagoya, Japan
[2]Department of Gastroenterology, Nagoya City Koseiin Medical Welfare Center, Nagoya, Japan
[3]Department of Gastroenterology and Metabolism, Nagoya City University Graduate School of Medical Sciences, Nagoya, Japan
[4]Department of Therapeutic Research, National Hospital Organization (NHO) Nagasaki Medical Center, Nagasaki, Japan
[5]The Research Center for Hepatitis and Immunology, National Center for Global Health and Medicine, Ichikawa, Japan
[6]PhoenixBio Co. Ltd., Higashi-Hiroshima, Japan
[7]Tokyo Metropolitan Institute of Medical Science, Tokyo, Japan

Correspondence to
Dr Masashi Mizokami, The Research Center for Hepatitis and Immunology, National Center for Global Health and Medicine 1–7–1, Kohnodai, Ichikawa 272–8516, Japan; mmizokami@hospk.ncgm.go.jp

Revised 4 October 2012
Accepted 9 October 2012

ABSTRACT

Objective Recent studies have demonstrated that genetic polymorphisms near the *IL28B* gene are associated with the clinical outcome of pegylated interferon α (peg-IFN-α) plus ribavirin therapy for patients with chronic hepatitis C virus (HCV). However, it is unclear whether genetic variations near the *IL28B* gene influence hepatic interferon (IFN)-stimulated gene (ISG) induction or cellular immune responses, lead to the viral reduction during IFN treatment.

Design Changes in HCV-RNA levels before therapy, at day 1 and weeks 1, 2, 4, 8 and 12 after administering peg-IFN-α plus ribavirin were measured in 54 patients infected with HCV genotype 1. Furthermore, we prepared four lines of chimeric mice having four different lots of human hepatocytes containing various single nucleotide polymorphisms (SNP) around the *IL28B* gene. HCV infecting chimeric mice were subcutaneously administered with peg-IFN-α for 2 weeks.

Results There were significant differences in the reduction of HCV-RNA levels after peg-IFN-α plus ribavirin therapy based on the *IL28B* SNP rs8099917 between TT (favourable) and TG/GG (unfavourable) genotypes in patients; the first-phase viral decline slope per day and second-phase slope per week in TT genotype were significantly higher than in TG/GG genotype. On peg-IFN-α administration to chimeric mice, however, no significant difference in the median reduction of HCV-RNA levels and the induction of antiviral ISG was observed between favourable and unfavourable human hepatocyte genotypes.

Conclusions As chimeric mice have the characteristic of immunodeficiency, the response to peg-IFN-α associated with the variation in *IL28B* alleles in chronic HCV patients would be composed of the intact immune system.

Significance of this study

What is already known on this subject?

- Genetic polymorphisms near the *IL28B* gene are associated with a chronic HCV treatment response.
- HCV-infected patients with the *IL28B* homozygous favourable allele had a more rapid decline in HCV kinetics in the first and second phases by peg-IFN-α-based therapy.
- During the acute phase of HCV infection, a strong immune response among patients with the *IL28B* favourable genotype could induce more frequent spontaneous clearance of HCV.

What are the new findings?

- In chronically HCV genotype 1b-infected chimeric mice that have the characteristic of immunodeficiency, no significant difference in the reduction in serum HCV-RNA levels and the induction of antiviral hepatic ISG by the administration of peg-IFN-α was observed between favourable and unfavourable human hepatocyte *IL28B* genotypes.
- By comparison of serum HCV kinetics between human and chimeric mice, the viral decline in both the first and second phases by peg-IFN-α treatment was affected by the variation in *IL28B* genotypes only in chronic hepatitis C patients.

How might it impact on clinical practice in the foreseeable future?

- The immune response according to *IL28B* genetic variants could contribute to the first and second phases of HCV-RNA decline and might be critical for HCV clearance by peg-IFN-α-based therapy.

INTRODUCTION

Hepatitis C is a global health problem that affects a significant portion of the world's population. The WHO estimated that, in 1999, 170 million hepatitis C virus (HCV)-infected patients were present worldwide, with 3–4 million new cases appearing per year.[1]

The standard therapy for hepatitis C still consists of pegylated interferon-α (peg-IFN-α), administered once weekly, plus daily oral ribavirin for 24–48 weeks in countries where protease inhibitors are not available.[2] This combination therapy is quite successful in patients with HCV genotype 2 or 3 infection, leading to a sustained virological response (SVR) in approximately 80–90% of patients treated; however, in patients infected with HCV genotype 1 or 4, only approximately half of all treated individuals achieved a SVR.[3 4]

Table 1 Characteristics of 54 patients infected HCV genotype 1

	IL28B SNP rs8099917		
	TT (n=34)	TG (n=19) + GG (n=1)	p Value
Age (years)	55.6±10.1	54.7±11.3	0.746
Gender (male %)	70	50	0.199
Body mass index (kg/m^2)	24.6±3.1	24.7±3.3	0.870
Viral load at therapy (log IU/ml)	6.0±0.7	5.8±0.8	0.357
SVR rate (%)	50	11	0.012
Serum ALT level (IU/l)	100.3±80.8	79.3±45.0	0.226
Platelet count (×10^4/μl)	17.1±9.0	16.5±5.8	0.771
Fibrosis (F3+4 %)	42	40	0.877

HCV, hepatitis C virus; SNP, single nucleotide polymorphism; SVR, sustained virological response.

Host factors were shown to be associated with the outcome of the therapy, including age, sex, race, liver fibrosis and obesity.[5] Genome-wide association studies have demonstrated that genetic variations in the region near the interleukin-28B (*IL28B*) gene, which encodes interferon (IFN)-λ3, are associated with a chronic HCV treatment response.[6–10] Furthermore, it was demonstrated that genetic variations in the *IL28B* gene region are also associated with spontaneous HCV clearance.[11–12]

Interestingly, a recent report showed the effect of genetic polymorphisms near the *IL28B* gene on the dynamics of HCV during peg-IFN-α plus ribavirin therapy in Caucasian, African American and Hispanic individuals;[13] HCV-infected patients with the *IL28B* homozygous favourable allele had a more rapid decline of HCV in the first phase, which is associated with the inhibition of viral replication as well as the second phase associated with immuno-destruction of viral-infected hepatocytes.[14] However, it is unknown how a direct effect by the *IL28B* genetic variation, such as the induction of IFN-stimulated genes (ISG) or cellular immune responses, would influence the viral kinetics during IFN treatment. Over recent periods, engineered severe combined immunodeficient (SCID) mice transgenic for urokinase-type plasminogen activator (uPA) received human hepatocyte transplants (hereafter referred to as chimeric mice)[15–17] and are suitable for experiments with hepatitis viruses in vivo.[18 19] We have also reported that these chimeric mice carrying human hepatocytes are a robust animal model to evaluate the efficacy of IFN and other anti-HCV agents.[20 21]

The purpose of this study was to reveal the association between genetic variations in the *IL28B* gene region and viral decline during peg-IFN-α treatment in patients with HCV, and to clarify the association between different *IL28B* alleles of human hepatocytes in chimeric mice and the response to peg-IFN-α without immune response. These studies will elucidate whether the immune response by the *IL28B* genetic variation affects the viral kinetics during peg-IFN-α treatment.

MATERIALS AND METHODS

Patients

Fifty-four Japanese patients with chronic HCV genotype 1 infection at Nagasaki Medical Center and Nagoya City University were enrolled in this study (table 1). Patients received peg-IFN-α2a (180 μg) or 2b (1.5 μg/kg) subcutaneously every week and were administered a weight-adjusted dose of ribavirin (600 mg for <60 kg, 800 mg for 60–80 kg, and 1000 mg for >80 kg daily), which is the recommended dosage in Japan. Patients with other hepatitis virus infection or HIV coinfection were not included in the study. The study protocol conformed to the ethics guidelines of the 1975 Declaration of Helsinki as reflected by earlier approval by the institutions' human research committees.

Laboratory tests

Blood samples were obtained before therapy, as well as on day 1 and at weeks 1, 2, 4, 8 and 12 after the start of therapy and were analysed for the HCV-RNA level by the commercial Abbott Real-Time HCV test with a lower limit of detection of 12 IU/ml (Abbott Molecular Inc., Des Plains, Illinois, USA). Genetic polymorphism in the *IL28B* gene (rs8099917), a single nucleotide polymorphism (SNP) recently identified to be associated with treatment response,[6–8] was tested by the TaqMan SNP genotyping assay (Applied Biosystems, Foster City, California, USA).

HCV infection of chimeric mice with the liver repopulated for human hepatocytes

SCID mice carrying the uPA transgene controlled by an albumin promoter were injected with 5.0–7.5×10^5 viable hepatocytes through a small left-flank incision into the inferior splenic pole, thereafter chimeric mice were generated. The chimeric mice were purchased from PhoenixBio Co, Ltd (Hiroshima, Japan).[17] Human hepatocytes with the *IL28B* homozygous favourable allele, heterozygous allele or homozygous unfavourable allele were imported from BD Biosciences (San Jose, California, USA) (table 2). Murine serum levels of human albumin and the body weight were not significantly different among four chimeric mice groups, providing a reliable comparison for anti-HCV agents.[22] Three different serum samples were obtained from three chronic HCV patients (genotype 1b).[21 22] Each mouse was intravenously infected with serum sample containing 10^5 copies of HCV genotype 1b. Administration of peg-IFN-α2a (Pegasys; Chugai Pharmaceutical Co., Ltd., Tokyo, Japan) at the dose formulation (30 μg/kg) was consecutively applied to each mouse on days 0, 3, 7 and 10 (table 3).

HCV-RNA quantification

HCV-RNA in mice sera (days 0, 1, 3, 7 and 14) was quantified by an in-house real-time detection PCR assay with a lower quantitative limit of detection of 10 copies/assay, as previously reported.[21]

Quantification of IFN-stimulated gene-expression levels

For analysis of endogenous ISG levels, total RNA was isolated from the liver using the RNeasy RNA extraction kit (Qiagen, Valencia, California, USA) and complementary DNA synthesis

Table 2 Four lines of uPA/SCID mice from four different lots of human hepatocytes (donor) containing various SNP around the *IL28B* gene

uPA/SCID mice	Donor	Race	Age	Gender	rs8103142	rs12979860	rs8099917
PXB mice	A	African American	5 Years	Male	CC	TT	TG
	B	Caucasian	10 Years	Female	CC	TT	TG
	C	Hispanic	2 Years	Female	TT	CC	TT
	D	Caucasian	2 Years	Male	TT	CC	TT

PXB mice; urokinase-type plasminogen activator/severe combined immunodeficiency (uPA/SCID) mice repopulated with approximately 80% human hepatocytes.
SCID, severe combined immunodeficient; SNP, single nucleotide polymorphism.

Gut 2012;**0**:1–7. doi:10.1136/gutjnl-2012-302553

Table 3 Dosage and time schedule of pegIFN-α2a* treatment for HCV genotype 1b infected chimeric mice

Donor hepatocytes†	No of chimeric mice	Inoculum	Test compound	Dose			
				Level (μg/kg)	Concentrtion (μg/ml)	Volume (ml/kg)	Frequency
A	3	Serum A	Peg-IFN-α2a	30	3	10	Day 0, 3, 7, 10
B	4	Serum A	Peg-IFN-α2a	30	3	10	Day 0, 3, 7, 10
C	3	Serum A	Peg-IFN-α2a	30	3	10	Day 0, 3, 7, 10
D	3	Serum A	Peg-IFN-α2a	30	3	10	Day 0, 3, 7, 10
A	2	Serum B	Peg-IFN-α2a	30	3	10	Day 0, 3, 7, 10
C	2	Serum B	Peg-IFN-α2a	30	3	10	Day 0, 3, 7, 10
A	2	Serum C	Peg-IFN-α2a	30	3	10	Day 0, 3, 7, 10
C	2	Serum C	Peg-IFN-α2a	30	3	10	Day 0, 3, 7, 10

*Pegasys; Chugai Pharmaceutical Co., Ltd., Tokyo, Japan.
†The *IL28B* genetic variation of the donor hepatocytes was indicated in table 2.
HCV, hepatitis C virus; peg-IFN-α, pegylated interferon α.

was performed using 2.0 μg of total RNA (High Capacity RNA-to-cDNA kit; Applied Biosystems). Fluorescence real-time PCR analysis was performed using an ABI 7500 instrument (Applied Biosystems) and TaqMan Fast Advanced gene expression assay (Applied Biosystems). TaqMan Gene Expression Assay primer and probe sets (Applied Biosystems) are shown in the supplementary information (available online only). Relative amounts of messenger RNA, determined using a FAM-Labeled TaqMan probe, were normalised to the endogenous RNA levels of the housekeeping reference gene, glyceraldehyde-3-phosphate dehydrogenase. The delta Ct method ($2^{-(\text{delta Ct})}$) was used for quantitation of relative mRNA levels and fold induction.[23 24]

Statistical analyses

Statistical differences were evaluated by Fisher's exact test or the χ^2 test with the Yates correction. Mice serum HCV-RNA and intrahepatic ISG expression levels were compared using the Mann–Whitney U test. Differences were considered significant if p values were less than 0.05.

RESULTS

Characteristics of the study patients

Genotypes (rs8099917) TT, TG and GG were detected in 34, 19 and one patient infected with HCV genotype 1, respectively. SVR rates were significantly higher in HCV patients with genotype TT than in those with genotype TG/GG (50% vs 11%, p=0.012). The initial HCV serum load was comparable between genotypes TT and TG/GG (6.0±0.7 vs 5.8±0.8 log IU/ml). There were no significant differences in sex (male%, 70% vs 50%), age (55.6±10.1 vs 54.7±11.3 years), serum alanine aminotransferase level (100.3±80.8 vs 79.3±45.0 IU/L), platelet count (17.1±9.0 vs 16.5±5.8×10^4/μl) and fibrosis stages (F3/4%, 42% vs 40%) between HCV patients with the favourable (rs8099917 TT) and unfavourable (rs8099917 TG/GG) *IL28B* genotypes (table 1).

Changes in serum HCV-RNA levels in patients treated by peg-IFN-α plus ribavirin

Figure 1 shows the initial change in the serum HCV-RNA level for 14 days after peg-IFN-α plus ribavirin therapy in patients infected with HCV genotype 1 based on the genetic polymorphism near the *IL28B* gene. The immediate antiviral response (viral drop 24 h after the first IFN injection) was significantly higher in HCV patients with genotype TT than genotype TG/GG (−1.08 vs −0.39 log IU/ml, p<0.001). Figure 2 also shows the subsequent change in the serum HCV-RNA reduction after peg-IFN-α plus ribavirin therapy in patients infected with HCV genotype 1. Similarly, during peg-IFN-α plus ribavirin therapy, a statistically significant difference in the median reduction in serum HCV-RNA levels was noted according to the genotype (TT vs TG/GG). The median reduction in the serum HCV-RNA levels (log IU/ml) at 1, 2, 4, 8 and 12 weeks between genotypes TT and TG/GG was as follows: −1.58 vs −0.62, p<0.001; −2.35 vs −0.91, p<0.001;

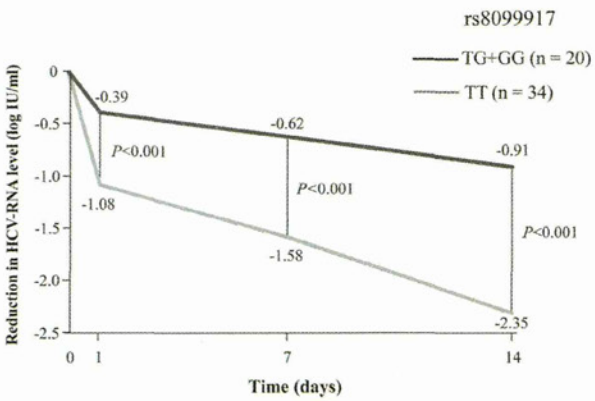

Figure 1 Rapid reduction of median hepatitis C virus (HCV)-RNA levels (log IU/ml) at 1, 7 and 14 days between *IL28B* single nucleotide polymorphisms rs8099917 genotype TT (n=34) and TG/GG (n=20) in HCV genotype 1-infected patients treated with peg-IFN-α plus ribavirin.

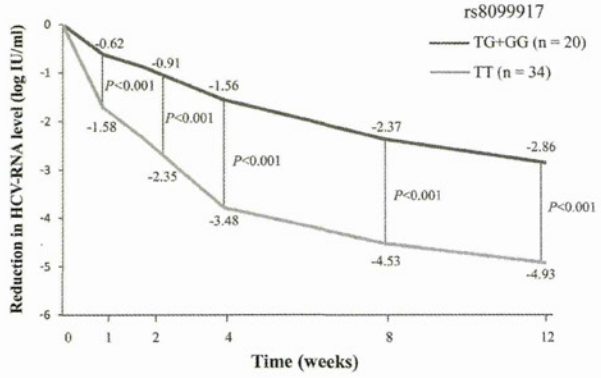

Figure 2 Weekly reduction of median hepatitis C virus (HCV)-RNA levels (log IU/ml) at 1, 2, 4, 8 and 12 weeks between *IL28B* single nucleotide polymorphisms rs8099917 genotype TT (n=34) and TG/GG (n=20) in HCV genotype 1-infected patients treated with pegylated interferon α plus ribavirin.

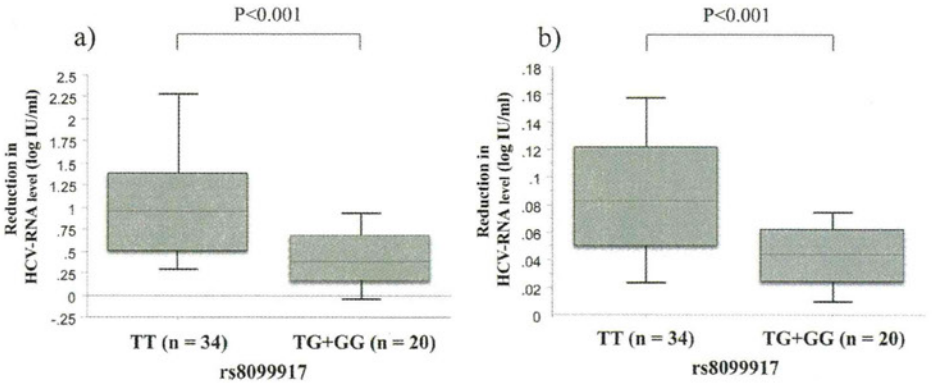

Figure 3 (A) The first-phase viral decline slope per day (Ph1/day) and (B) second-phase viral decline slope per week (Ph2/week) in hepatitis C virus (HCV) genotype 1-infected patients treated with pegylated interferon α plus ribavirin. The lines across the boxes indicate the median values. The hash marks above and below the boxes indicate the 90th and 10th percentiles for each group, respectively.

−3.48 vs −1.56, p<0.001; −4.53 vs −2.37, p<0.01; −4.93 vs −2.86, p<0.001. Furthermore, the initial first-phase viral decline slope per day (Ph1/day) and subsequent second-phase viral decline slope per week (Ph2/week) in TT genotype were significantly higher than in genotype TG/GG (Ph1/day 0.94 ±0.83 vs 0.38±0.40 log IU/ml, p<0.001; Ph2/week 0.08±0.06 vs 0.04±0.03 log IU/ml, p<0.001) (figure 3).

Changes in serum HCV-RNA levels in chimeric mice treated by peg-IFN-α

In order to clarify the association between *IL28B* alleles of human hepatocytes and the response to peg-IFN-α, we prepared four lines of uPA/SCID mice and four different lots of human hepatocytes containing various rs8099917, rs8103142 and rs12979860 SNPs around the *IL28B* gene (table 2). The chimeric mice were inoculated with serum samples from each HCV-1b patient, and then HCV-RNA levels had increased and reached more than 10^6 copies/ml in all chimeric mice sera at 2 weeks after inoculation. After confirming the peak of HCV-RNA in all chimeric mice, they were subcutaneously administered with four times injections of the bolus dose of peg-IFN-α2a for 2 weeks (table 3). Figure 4 shows the change in the serum HCV-RNA levels for 14 days during IFN injection into chimeric mice transplanted with *IL28B* favourable or unfavourable human hepatocyte genotypes. On peg-IFN-α administration, no significant difference in the median reduction in HCV-RNA levels in the serum A-infected[22] chimeric mice sera was observed between favourable (n=7) and unfavourable

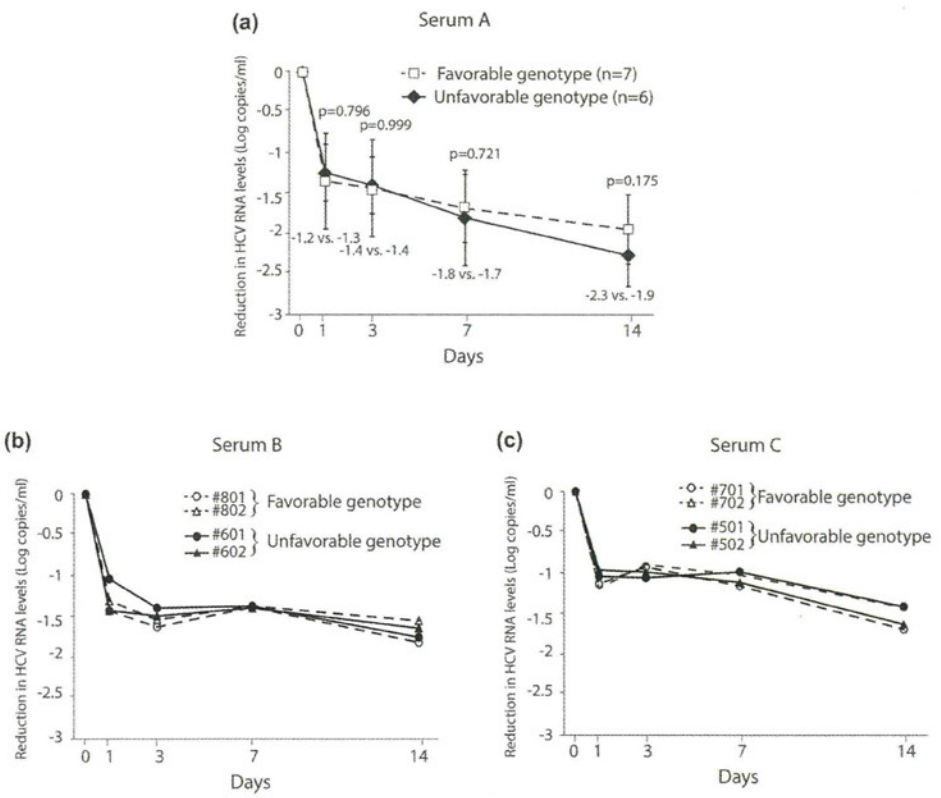

Figure 4 Median reduction of hepatitis C virus (HCV)-RNA levels (log copies/ml) after administering pegylated interferon α to chimeric mice having human hepatocytes containing various single nucleotide polymorphisms around the *IL28B* gene as favourable (rs8099917 TT) and unfavourable (rs8099917 TG) genotypes. Data are represented as mean+SD. Chimeric mice infected with a) serum A (n=7; favourable genotype, n=6; unfavourable genotype), (B) serum B (n=2, each genotype), and (C) serum C (n=2, each genotype). All serum samples were obtained from HCV-1b patients.

(n=6) *IL28B* genotypes on days 1, 3, 7 and 14 (−1.2 vs −1.3, −1.4 vs −1.4, −1.8 vs −1.7, and −2.3 vs −1.9 log copies/ml) (figure 4A). Moreover, we prepared two additional serum samples from the other HCV-1b patients (serum B and C)[21] to confirm the influence of *IL28B* genotype in early viral kinetics during IFN treatment. After establishing persistent infection with new HCV-1b strains in all chimeric mice, they were also administered four times injections of the bolus dose of peg-IFN-α2a for 2 weeks (figure 4B,C). In a similar fashion, no significant difference in HCV-RNA reduction in chimeric mice sera was observed between favourable and unfavourable *IL28B* genotypes.

Expression levels of ISG in chimeric mice livers

Because chimeric mice have the characteristic of severe combined immunodeficiency, the viral kinetics in chimeric mice sera during IFN treatment could be contributed by the innate immune response of HCV-infected human hepatocytes. Therefore, ISG expression levels in mice livers transplanted with human hepatocytes were compared between favourable and unfavourable *IL28B* genotypes (figure 5).

As shown in figure 5A, ISG expression levels in mice livers were measured at 8 h and 24 h after IFN treatment. The levels of representative antiviral ISG (eg, myxovirus resistance protein A, oligoadenylate synthetase 1, RNA-dependent protein kinase) and other ISG for promoting antiviral signalling (eg, Toll-like receptor 3, retinoic acid-inducible gene 1) were significantly induced at least 8 h after treatment, and prolonged at 24 h. No significant difference in ISG expression levels in HCV-infected livers was observed between favourable and unfavourable *IL28B* genotypes. The other inoculum for persistent infection of HCV-1b also demonstrated no significant difference in ISG

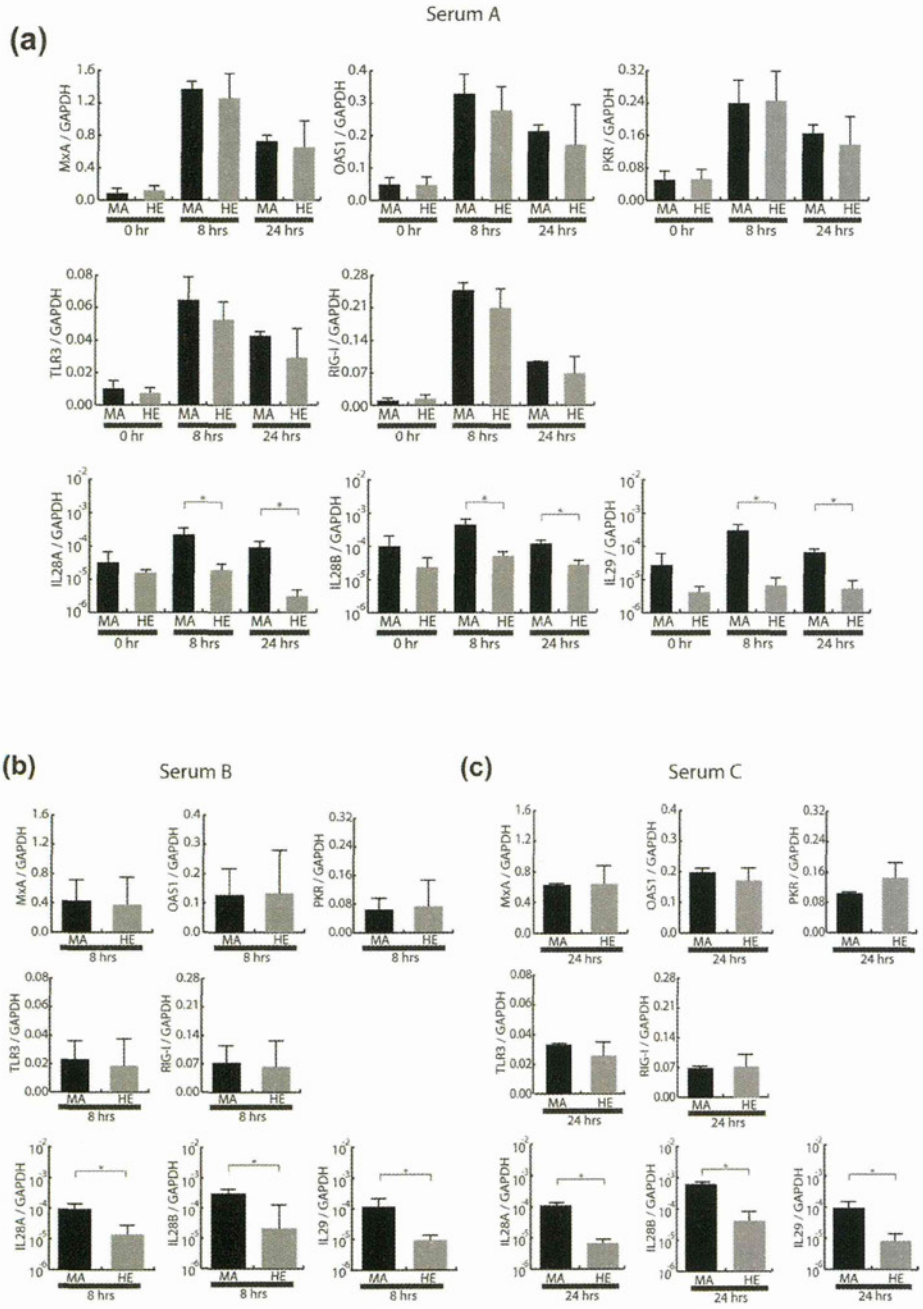

Figure 5 Intrahepatic interferon (IFN)-stimulated gene (ISG) expression levels in the pegylated interferon α (peg-IFN-α)-treated chimeric mice having human hepatocytes containing homozygous favourable allele (rs8099917 TT; MA) and heterozygous unfavourable allele (rs8099917 TG; HE) were measured and expressed relative to glyceraldehyde-3-phosphate dehydrogenase (GAPDH) messenger RNA. Data are represented as mean+SD. (A) Time kinetics of ISG after administration of the peg-IFN-α in serum A-infected chimeric mice (n=3, each genotype). Comparison of ISG expression levels at (B) 8 h in serum B-infected mice and (C) 24 h in serum C-infected mice after administering peg-IFN-α (n=3, each genotype). Predesigned real-time PCR assay of IL28B transcript purchased from Applied Biosystems can be cross-reactive to IL28A transcript. *p<0.05. MxA, myxovirus resistance protein A; OAS1, oligoadenylate synthetase 1; PKR, RNA-dependent protein kinase; RIG-1, retinoic acid-inducible gene 1; TLR3, Toll-like receptor 3.

expression levels between favourable and unfavourable *IL28B* genotypes (figure 5B,C). Interestingly, IFN-λ expression levels by treatment of peg-IFN-α were significantly induced in HCV-infected human hepatocytes harbouring the favourable *IL28B* genotype (figure 5 A–C).

DISCUSSION

Several recent studies have demonstrated a marked association between the chronic hepatitis C treatment response[6–9] and SNP (rs8099917, rs8103142 and rs12979860) near or within the region of the *IL28B* gene, which affected the viral dynamics during peg-IFN-α plus ribavirin therapy in Caucasian, African American and Hispanic individuals.[13]

It has been reported that when patients with chronic hepatitis C are treated by IFN-α or peg-IFN-α plus ribavirin, HCV-RNA generally declines after a 7–10 h delay.[25] The typical decline is biphasic and consists of a rapid first phase lasting for approximately 1–2 days during which HCV-RNA may fall 1–2 logs in patients infected with genotype 1, and subsequently a slower second phase of HCV-RNA decline.[26] The viral kinetics had a predictive value in evaluating antiviral efficacy.[14] In this study, biphasic decline of the HCV-RNA level during peg-IFN-α treatment was observed in both patients and chimeric mice infected with HCV genotype 1; however, in the first and second phases of viral kinetics, a difference between *IL28B* genotypes was observed only in HCV-infected patients; a more rapid decline in serum HCV-RNA levels after administering peg-IFN-α plus ribavirin was confirmed in patients with the TT genotype of rs8099917 compared to those with the TG/GG genotype.

On the other hand, in-vivo data using the chimeric mouse model showed no significant difference in the reduction of HCV-RNA titers in mouse serum among four different lots of human hepatocytes containing *IL28B* favourable (rs8099917 TT) or unfavourable (rs8099917 TG) genotypes, which was confirmed by the inoculation of two additional HCV strains. These results indicated that variants of the *IL28B* gene in donor hepatocytes had no influence on the response to peg-IFN-α under immunosuppressive conditions, suggesting that the immune response according to *IL28B* genetic variants could contribute to the first and second phases of HCV-RNA decline and might be critical for HCV clearance by peg-IFN-α-based therapy.

Two recent studies indeed revealed an association between the *IL28B* genotype and the expression level of hepatic ISG in human studies.[27 28] Quiescent hepatic ISG before treatment among patients with the *IL28B* favourable genotype have been associated with sensitivity to exogenous IFN treatment and viral eradication; however, it is difficult to establish whether the hepatic ISG expression level contributes to viral clearance independently or appears as a direct consequence of the *IL28B* genotype. Another recent study addressed this question and the results suggested that there is no absolute correlation with the *IL28B* genotype and hepatic expression of ISG.[29] Our results on the hepatic ISG expression level in immunodeficient chimeric mice also suggested that no significant difference in ISG expression levels was observed between favourable and unfavourable *IL28B* genotypes. However, these results were not consistent with a previous report using chimeric mice that the favourable *IL28B* genotype was associated with an early reduction in HCV-RNA by ISG induction.[30] The reasons for the discrepancy might depend on the dose and type of IFN treatment, as well as the time point when ISG expression was examined in the liver. In addition, although IFN-λ transcript levels measured in peripheral blood mononuclear cells or liver revealed inconsistent results in the context of an association with the *IL28B* genotype,[7 8] our preliminary assay on the IL28A, IL28B and IL29 transcripts in the liver first indicated that the induction of IFN-λ on peg-IFN-α administration could be associated with the *IL28B* genotype. Therefore, the induction of IFN-λ followed by immune response might contribute to different viral kinetics and treatment outcomes in HCV-infected patients, because no difference was found in chimeric mice without immune response.

It has also been reported that the mechanism of the association of genetic variations in the *IL28B* gene and spontaneous clearance of HCV may be related to the host innate immune response.[11] Interestingly, participants with seroconversion illness with jaundice were more frequently rs8099917 homozygous favourable allele (TT) than other genotypes (32% vs 5%, p=0.047). This suggests that a stronger immune response during the acute phase of HCV infection among patients with the *IL28B* favourable genotype would induce more frequent spontaneous clearance of HCV.

Taking into account both the above results in acute HCV infection and our results conducted on chimeric mice that have the characteristic of immunodeficiency, it is suggested that the response to peg-IFN-α associated with the variation in *IL28B* alleles in chronic hepatitis C patients would be composed of the intact immune system.

Acknowledgements The authors would like to thank Kyoko Ito of Nagoya City University Graduate School of Medical Sciences, Nagoya, Japan for doing the quantification of gene-expression assays.

Contributors YT and MM conceived the study. TW and FS and YT conducted the study equally. TW and FS coordinated the analysis and manuscript preparation. All the authors had input into the study design, patient recruitment and management or mouse management and critical revision of the manuscript for intellectual content. TW, FS and YT contributed equally.

Funding This study was supported by a grant-in-aid from the Ministry of Health, Labour, and Welfare of Japan (H22-kannen-005) and the Ministry of Education, Culture, Sports, Science and Technology, Japan, and grant-in-aid for research in Nagoya City University.

Competing interests None.

Patient consent Obtained.

Ethics approval This study was conducted with the approval of each ethics committee at the Nagoya City University and Nagasaki Medical Center (see supplementary information, available online only).

Provenance and peer review Not commissioned; externally peer reviewed.

REFERENCES

1. **Ray Kim W.** Global epidemiology and burden of hepatitis C. *Microbes Infect* 2002;**4**:1219–25.
2. **Foster GR.** Past, present, and future hepatitis C treatments. *Semin Liver Dis* 2004;**24**(Suppl. 2):97–104.
3. **Fried MW,** Shiffman ML, Reddy KR, *et al*. Peginterferon alfa-2a plus ribavirin for chronic hepatitis C virus infection. *N Engl J Med* 2002;**347**:975–82.
4. **Manns MP,** McHutchison JG, Gordon SC, *et al*. Peginterferon alfa-2b plus ribavirin compared with interferon alfa-2b plus ribavirin for initial treatment of chronic hepatitis C: a randomised trial. *Lancet* 2001;**358**:958–65.
5. **Mihm U,** Herrmann E, Sarrazin C, *et al*. Review article: predicting response in hepatitis C virus therapy. *Aliment Pharmacol Ther* 2006;**23**:1043–54.
6. **Ge D,** Fellay J, Thompson AJ, *et al*. Genetic variation in IL28B predicts hepatitis C treatment-induced viral clearance. *Nature* 2009;**461**:399–401.
7. **Suppiah V,** Moldovan M, Ahlenstiel G, *et al*. IL28B is associated with response to chronic hepatitis C interferon-alpha and ribavirin therapy. *Nat Genet* 2009;**41**:1100–4.
8. **Tanaka Y,** Nishida N, Sugiyama M, *et al* Genome-wide association of IL28B with response to pegylated interferon-alpha and ribavirin therapy for chronic hepatitis C. *Nat Genet* 2009;**41**:1105–9.
9. **Rauch A,** Kutalik Z, Descombes P, *et al*. Genetic variation in IL28B is associated with chronic hepatitis C and treatment failure: a genome-wide association study. *Gastroenterology* 2010;**138**:1338–45.